HHS Public Access

Author manuscript

Cell Rep. Author manuscript; available in PMC 2023 August 20.

Published in final edited form as:

Cell Rep. 2023 July 25; 42(7): 112717. doi:10.1016/j.celrep.2023.112717.

Muscle-building supplement β-hydroxy β-methylbutyrate binds to PPARα to improve hippocampal functions in mice

Ramesh K. Paidi[1], **Sumita Raha**[1], **Avik Roy**[2], **Kalipada Pahan**[1,3,4,*]

[1]Department of Neurological Sciences, Rush University Medical Center, Chicago, IL, USA

[2]Simmaron Research Institute, Technology Innovation Center, 10437 W Innovation Drive, Wauwatosa, WI, USA

[3]Division of Research and Development, Jesse Brown Veterans Affairs Medical Center, Chicago, IL, USA

[4]Lead contact

SUMMARY

This study underlines the importance of β-hydroxy β-methylbutyrate (HMB), a muscle-building supplement in human, in increasing mouse hippocampal plasticity. Detailed proteomic analyses reveal that HMB serves as a ligand of peroxisome proliferator-activated receptor α (PPARα), a nuclear hormone receptor involved in fat metabolism, via interaction with the Y314 residue. Accordingly, HMB is ineffective in increasing plasticity of $PPARα^{-/-}$ hippocampal neurons. While lentiviral establishment of full-length PPARα restores the plasticity-promoting effect of HMB in $PPARα^{-/-}$ hippocampal neurons, lentiviral transduction of Y314D-PPARα remains unable to do that, highlighting the importance of HMB's interaction with the Y314 residue. Additionally, oral HMB improves spatial learning and memory and reduces plaque load in 5X familial Alzheimer's disease (*5XFAD*) mice, but not in $5XFAD^{\Delta PPARα}$ mice (*5XFAD* lacking PPARα), indicating the involvement of PPARα in HMB-mediated neuroprotection in *5XFAD* mice. These results delineate neuroprotective functions of HMB and suggest that this widely used supplement may be repurposed for AD.

In brief

HMB is a muscle-building supplement in human. Paidi et al. demonstrate that HMB binds to PPARα to increase hippocampal functions. Moreover, oral HMB protects cognitive functions and reduces plaques in a mouse model of Alzheimer's disease (AD) via PPARα, indicating a possible beneficial effect of HMB in AD.

*Correspondence: kalipada_pahan@rush.edu.

AUTHOR CONTRIBUTIONS

K.P. conceived the original idea, supervised the project, acquired the funding, and wrote the manuscript. R.K.P. and K.P. designed the study. R.K.P., S.R., and A.R. performed the research. R.K.P., S.R., A.R., and K.P. analyzed the data.

DECLARATION OF INTERESTS

The authors declare no competing interests.

SUPPLEMENTAL INFORMATION

Supplemental information can be found online at https://doi.org/10.1016/j.celrep.2023.112717.

Graphical Abstract

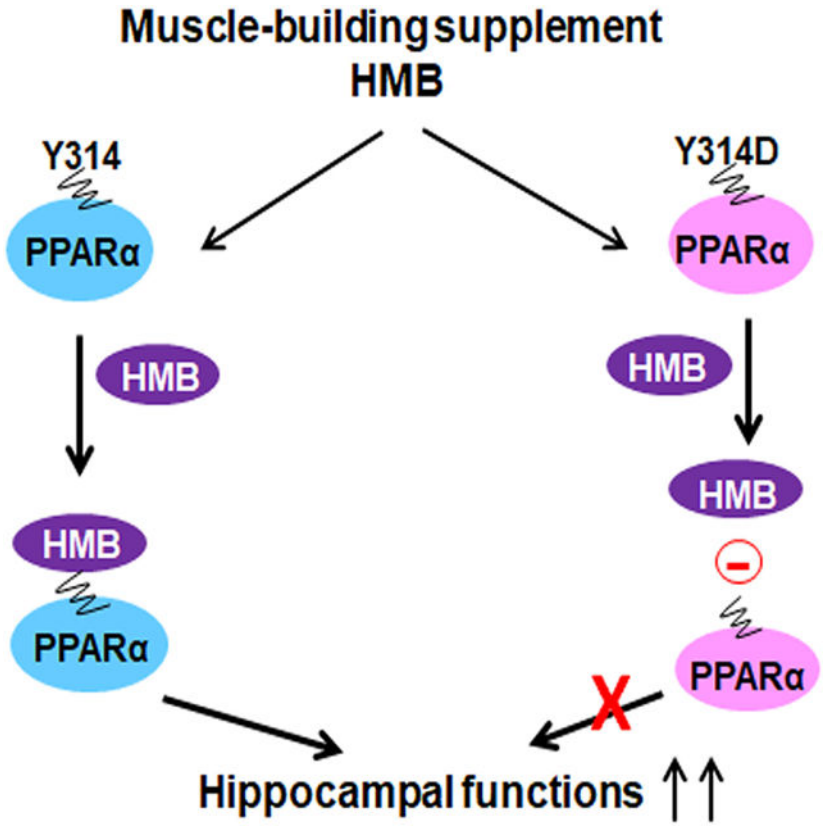

INTRODUCTION

Alzheimer's disease (AD) is the most common human neurodegenerative disorder, comprising almost two-thirds of all cases of dementia.[1] For patients with AD, usually the first clinical sign appears after age 60. Although the etiology of AD is poorly understood, it is now well established that AD is a multifactorial disease of the brain involving lifestyle, genetic, and environmental factors.[2,3] Senile plaques, neurofibrillary tangles, and neuronal loss are classical pathological features of AD. However, synapse loss is believed to be a profound neuropathology of AD, and accordingly, from a clinical angle, it is identified by progressive impairment in memory, judgment, decision-making, and language usage.[4] It has been reported that individuals with early AD have significantly fewer synapses than those with mild cognitive impairment (MCI) and no cognitive impairment (NCI) and that the number of synapses exhibits a significant correlation with the subject's Mini-Mental State scores.[5] Interestingly, synaptic loss does not display any relationship to either Braak stage or apoE genotype.[5] Therefore, promotion of hippocampal plasticity is an important area of research, as it may help in the preservation of memory in healthy brains and improvement in cognitive functions in individuals with AD and MCI.

Body builders regularly use β-hydroxy β-methylbutyrate (HMB) as a muscle-building supplement to increase exercise-induced gains in muscle size and muscle strength and

improve exercise performance. HMB is a very safe supplement, and even after long-term use, it does not exhibit any side effects. Here, we describe that HMB is endowed with a unique property of stimulating hippocampal plasticity. Although HMB is widely used among athletes and body builders as an ergogenic aid, nothing was known about its receptor.

Although the liver is rich in peroxisome proliferator-activated receptor α (PPARα), a nuclear hormone receptor known to participate in fatty acid metabolism,[6,7] we have seen the presence of PPARα in the hippocampus, which is involved in spatial learning and memory via activation of cAMP response element-binding protein (CREB).[8–11] Here, we found that HMB interacted with the ligand-binding domain of PPARα to activate PPARα and promote hippocampal functions. Accordingly, oral administration of low-dose HMB increased the AMPA- and NMDA-mediated calcium current in hippocampal slices and enhanced memory and learning in 5X familial AD (*5XFAD*) mice but not *5XFAD* mice lacking *PPARα* (*5XFAD*$^{\Delta PPAR\alpha}$). Furthermore, HMB treatment lowered plaque load in *5XFAD*, but not in *5XFAD*$^{\Delta PPAR\alpha}$, mice. These results suggest HMB may be beneficial for patients with AD via PPARα-mediated neuroprotection.

RESULTS

Upregulation of morphological plasticity in hippocampal neurons by HMB

Since the hippocampus, a vital module of memory circuit of the medial temporal lobe, is affected early in AD to display synaptic abnormality, it is believed that upregulation of hippocampal plasticity may be beneficial for AD and other cognitive disorders.[12–14] HMB is a widely used muscle-building supplement, and to understand the effect of HMB on hippocampal plasticity, at first, we examined morphological plasticity. Since dendritic spines are the major sites of excitatory synaptic transmission in the CNS, and accordingly, the functioning of neuronal circuits is influenced by the size and density of dendritic spines,[15,16] we monitored the status of dendritic spines. Interestingly, HMB treatment significantly increased the density of spines (Figures 1A–1C) in primary mouse hippocampal neurons. We further confirmed these observations by quantifying spine size. Similar to the increase in spine density, HMB treatment also augmented spine size in primary hippocampal neurons (Figure 1D). NMDA receptor subunit NR-2A[17] and AMPA-receptor subunit GluR1[18] are some of the major plasticity-related molecules in the hippocampus. As is evident from immunofluorescence analysis (Figures 1E and 1F), HMB treatment markedly increased the levels of NR2A and GluR1 in primary hippocampal neurons. This was also supported by mean fluorescence intensity (MFI) analysis of NR2A (Figure 1G) and GluR1 (Figure 1H). Several studies have established that calcium influx through NMDA- and AMPA-type glutamate receptors regulates diverse processes including kinase and phosphatase activities, protein trafficking, structural and functional synaptic plasticity, cell growth, cell survival, and apoptosis.[19–21] Therefore, next, we examined whether HMB could arouse the calcium influx in cultured hippocampal neurons. Interestingly, both AMPA (Figure 1I) and NMDA (Figure 1J) elicited a stronger calcium influx following HMB treatment. Since we recorded the NMDA-driven calcium currents in the presence of AMPA-antagonist Naspm (Figure 1I) and AMPA-driven (Figure 1J) calcium currents in the presence of NMDA receptor blocker

N20C in HMB-treated primary hippocampal neurons, these results already nullified the contribution of passive calcium currents.

VanGuilder et al.[22] have reported that a decrease in positive clusters for PSD95, an indicator of loss of actual synapses, positively correlates with cognitive decline. Consistent to synaptic degeneration in AD, it has been also shown that the level of synaptosome-associated protein 25 (SNAP25) is significantly lower in AD brains and higher in cerebrospinal fluid (CSF) of subjects with AD.[23] BDNF is probably the most studied neurotrophin from the hippocampus that is known to regulate many of the hippocampus-based biological processes including hippocampal plasticity.[24,25] On the other hand, being the master regulator of memory and learning, CREB is known to control different plasticity-related molecules like NR-2A, GluR1, PSD95, BDNF, etc., at the transcriptional level.[10,26] Therefore, we also monitored PSD95, SNAP25, BDNF, and CREB in HMB-treated hippocampal neurons. Interestingly, HMB stimulated the levels of PSD95 (Figures S1A and S1E), SNAP25 (Figures S1B and S1F), BDNF (Figures S1C and S1G), and CREB (Figures S1D and S1H) in hippocampal neurons. These results suggest that HMB is capable of increasing the density of dendritic spines and enhancing the levels of plasticity-related molecules in cultured hippocampal neurons.

Oral administration of HMB upregulates hippocampal functions in 5XFAD mice

Since HMB improves morphological plasticity in cultured hippocampal neurons, next, we examined the effect of HMB *in vivo* in the hippocampus of *5XFAD* mice. At first, we examined whether after oral administration, HMB could enter into the brain. Three days after oral treatment at a dose of 5 mg/kg body weight (wt)/day, HMB was detected in the hippocampus of HMB-fed mice compared with control untreated mice (Figures S2A–S2C), indicating that HMB is capable of crossing the blood-brain barrier. Therefore, after 1 month of HMB treatment via gavage, the ionotropic calcium influx through NMDA and AMPA receptors was monitored in hippocampal slices. As reported earlier,[8,16] AMPA- (Figure 2A) and NMDA-dependent (Figure 2B) calcium influx as measured in organotypic hippocampal slices was less in *5XFAD* mice compared with age-matched non-transgenic (Tg) mice. However, consistent with the increase in calcium current in cultured hippocampal neurons, oral administration of HMB upregulated AMPA- (Figure 2A) and NMDA-driven (Figure 2B) calcium influx in the hippocampus of *5XFAD* mice.

Accordingly, double-label immunofluorescence of hippocampal sections revealed that the level of PSD95 (Figures 2C and 2D) and SNAP25 (Figures S3A and S3B) decreased in the hippocampus of *5XFAD* mice compared with non-Tg mice and that HMB feeding upregulated the expression of PSD95 (Figures 2C and 2D) and SNAP25 (Figures S3A and S3B) in the hippocampus of *5XFAD* mice. These results were confirmed by western blot analysis of hippocampal extracts with antibodies against PSD95 (Figure 2E) and SNAP25 (Figures S3C) followed by quantification of PSD95 (Figure 2F) and SNAP25 (Figure S3D). As expected, consistent with PSD95 and SNAP25, levels of BDNF (Figures S4A and S4D), total CREB (Figures S4B and S4E), and phosphorylated (phospho)-CREB (Figures S4C and S4F) also decreased in the hippocampus of *5XFAD* mice compared with non-Tg mice. However, oral HMB restored/upregulated BDNF (Figures S4A and S4D), total CREB

(Figures S4B and S4E), and phospho-CREB (Figures S4C and S4F) in the hippocampus of *5XFAD* mice. To confirm these findings further, we performed Golgi staining to visualize the status of dendritic spines in the hippocampus (Figures 2G–2I) by counting pedunculated spines (Figure 2J), non-pedunculated spines (Figure 2K), and total spines (Figure 2L) in the dendritic region of the hippocampal CA1 region. As expected, we found marked loss of pedunculated spines (Figure 2J), non-pedunculated spines (Figure 2K), and total spines (Figure 2L) in the hippocampus of *5XFAD* mice compared with non-Tg mice. However, oral HMB treatment restored/improved synaptic connections in the hippocampus of *5XFAD* mice as evident from Golgi-stained images (Figure 2I) and the numbers of pedunculated spines (Figure 2J), non-pedunculated spines (Figure 2K), and total spines (Figure 2L).

Next, we investigated the effect of HMB in improving hippocampus-dependent behaviors including memory and learning in *5XFAD* mice. The Barnes maze test is used to examine hippocampus-dependent spatial learning and memory.[10,11] As described before,[11,27] *5XFAD* mice exhibited diminished spatial behaviors shown by heatmap (Figure 2M), latency (Figure 2N), and errors (Figure 2O) compared with age-matched non-Tg mice. Similarly, *5XFAD* mice also performed poorly on T maze, in contrast to non-Tg mice, as demonstrated by positive turn (Figure 2P) and negative turn (Figure 2Q). However, at doses of 5 and 10 mg/kg/day, HMB markedly improved the performance of *5XFAD* mice on the Barnes maze (Figure 2M, heatmap; Figure 2N, latency; Figure 2O, errors) and T-maze (Figure 2P, positive turn; Figure 2Q, negative turn). HMB was more effective at a dose of 10 mg/kg/day than 5 mg/kg/day in improving cognitive functions of *5XFAD* mice (Figures 2M–2Q).

HMB binds to the ligand-binding domain of PPARα

Next, we wanted to delineate mechanisms by which HMB upregulates morphological plasticity of hippocampal neurons. Although liver is rich in PPARα, a lipid-lowering transcription factor, earlier, we have demonstrated that PPARα is present in the hippocampus and that PPARα also plays an important role in hippocampal plasticity.[9–11,28] Therefore, we examined the role of PPARα in this case. Double labeling of hippocampal sections with NeuN and PPARα showed a significant decrease in PPARα in the hippocampus of *5XFAD* mice compared with non-Tg mice (Figures S5A and S5B). However, oral HMB treatment markedly upregulated and/or normalized the level of PPARα in the hippocampus of *5XFAD* mice (Figures S5A and S5B). On the other hand, we did not see a decrease in PPARβ in the hippocampus of *5XFAD* mice compared with non-Tg mice (Figures S5C and S5D), and therefore HMB treatment also did not modulate the level of PPARβ in the hippocampus of *5XFAD* mice (Figures S5C and S5D), indicating the specificity of the effect.

Next, we were prompted to investigate the mechanisms of how HMB activates/increases PPARα and whether HMB could assist as a ligand of PPARα. SwissDock, a rigid body proteinligand docking tool, was employed to explore the interaction between HMB and ligand-binding domain (LBD) of PPARα at a molecular level. According to this analysis, we found that HMB docked in the ligand-binding pocket formed by Ser280, Y314, and H440 (Figures 3A, 3B, S6A, and S6B). To understand the importance of the ligand-binding pocket in the docking of HMB, a key residue of the pocket (Y314) was mutated to D314. When we

analyzed the interaction between HMB and Y314D PPARα, HMB was found to be posed far (>5 Å) from the ligand-binding pocket (Figure 3C). This was also reflected by total fitness energy, van der Waal energy, and total free energy (Figure S6C). However, *in silico* results need to be strengthened by experimental evidence. Therefore, we performed a time-resolved fluorescence resonance energy transfer (TR-FRET) assay[28] in order to validate the interaction between PPARα and HMB. As evident from Figure 3D, HMB indeed exhibited a strong interaction with PPARα. The binding curve resulted in an EC50 value of 3.35 nM with a Hill slope of 0.7710 (Figure 3D). This binding was almost comparable to that of a prototype activator of PPARα (gemfibrozil), which displayed an EC50 value of 4.02 nM with a Hill slope of 0.7949 (Figure 3E).

To further confirm the interaction between HMB and PPARα, we employed a thermal shift assay (TSA) of PPARα protein with 10 μM HMB. Briefly, full-length PPARα protein (FL-PPARα) was synthesized from HEK293FT cells transduced with lentiviral FL-PPARα. After that, its melting profile was monitored with the help of SYBR green reaction strategy at a range of 27°C–94°C. The typical sigmoidal melting curve clearly showed that our in-house recombinant FL-PPARα protein is conformationally stable (Figure 3F). Our TSA also revealed that 10 μM HMB strongly shifted the melting curve of FL-PPARα by 7C (Figure 3F). To confirm *in silico* results further, we also performed a TSA with Y314DPPARα protein, which showed that 10 μM HMB could shift the melting curve of Y314DPPARα by only 0.76C (Figure 3G), clearly indicating that HMB binds to the ligand-binding pocket of PPARα.

To confirm the functional significance of this finding, primary astrocytes isolated from *PPARα*$^{-/-}$ mice were transduced with *lenti-FL-PPARα* and *lenti-Y314D-PPARα* followed by HMB treatment. Consistent with structural and biophysical analyses, HMB treatment upregulated PPARα in *PPARα*$^{-/-}$ astrocytes (Figures 3H and 3I) that were transduced with *lenti-FL-PPARα*, but not *lenti-Y314D-PPARα*, further highlighting the importance of the interaction of HMB with the PPARα LBD in the activation of PPARα.

HMB-mediated upregulation of structural plasticity is dependent on its interaction with Y314 residue of PPARα

Next, we examined whether HMB augmented synaptic function via PPARα. Quantification of dendritic spine density is an important measure to evaluate hippocampal functions. Therefore, we employed a phalloidin-based quantification analysis of dendritic spines in HMB-treated hippocampal neurons. HMB increased spine density in wild-type (*WT*) (Figures 1A–1D), but not *PPARα*$^{-/-}$ (Figures 4A–4C), hippocampal neurons. Next, *PPARα*$^{-/-}$ hippocampal neurons were transduced with *lenti-FL-PPARα* for 2 days followed by overnight treatment with HMB. Interestingly, introduction of *FL-PPARα* significantly increased spine density in HMB-stimulated hippocampal neurons (Figures 4A and 4B). We further confirmed these observations by measuring spine size (Figure 4C) under the different treatment conditions. These results suggest that HMB upregulates morphological plasticity in hippocampal neurons via PPARα.

Along with the estimation of dendritic spine density, the measurement of calcium influx through ionotropic receptors including NMDA and AMPA receptors is considered another

reliable procedure to evaluate synaptic function.[19–21] Interestingly, HMB could not induce AMPA- and NMDA-driven calcium influx in cultured hippocampal neurons isolated from *PPARα*$^{-/-}$ mice (Figures 4D and 4E) compared with *WT* mice (Figures 1I and 1J), suggesting that HMB involves PPARα to upregulate calcium influx in hippocampal neurons. Next, to delineate a direct role of the Y314 residue of PPARα in HMB-induced calcium influx, *PPARα*$^{-/-}$ hippocampal neurons were transduced with *lenti-FL-PPARα* and *lenti-Y314DPPARα* for 2 days followed by stimulation with 10 μM HMB. Remarkably, HMB increased both AMPA- and NMDA-mediated calcium currents in *lenti-FL-PPARα*-transduced (Figures 4F and 4G), but not *lenti-Y314DPPARα*-transduced (Figures 4H and 4I), *PPARα*$^{-/-}$ hippocampal neurons. These results suggest that the binding of HMB with the Y314 residue of the PPARα LBD is important for HMBmediated upregulation of calcium influx in hippocampal neurons through NMDA- and AMPA-sensitive receptors.

HMB increases structural plasticity and protects memory and learning in 5XFAD mice via PPARα

Next, we investigated whether HMB required PPARα to protect hippocampal functions *in vivo* in mouse brain. Therefore, we used *5XFAD*$^{\Delta PPARα}$ mice (*5XFAD* mice lacking *PPARα*).[11,29] Seven-month-old *5XFAD*$^{\Delta PPARα}$ mice (n = 6) were fed with HMB for 30 days followed by monitoring of the ionotropic calcium influx through NMDA and AMPA receptors in hippocampal slices. In contrast to the upregulation of AMPA- and NMDAdependent calcium influx in organotypic hippocampal slices of *5XFAD* mice by HMB (Figures 2A and 2B), this supplement remained unable to stimulate calcium influx in hippocampal slices of *5XFAD*$^{\Delta PPARα}$ mice (Figures 5A and 5B). Although HMB treatment upregulated PSD95 in the hippocampus of *5XFAD* mice (Figures 2C–2F), an increase in PSD95 protein was not found in the hippocampus of HMB-treated *5XFAD*$^{\Delta PPARα}$ mice (Figures 5C–5F). Accordingly, oral HMB increased the level of SNAP25 in the hippocampus of *5XFAD* mice (Figures S3A–S3D) but not of *5XFAD*$^{\Delta PPARα}$ mice (Figures S7A–S7D). Similarly, HMB treatment also remained unable to increase the level of BDNF (Figures S8A and S8D), CREB (Figures S8B and S8E), and phospho-CREB (Figures S8C and S8F) in the hippocampus of *5XFAD*$^{\Delta PPARα}$ mice. These results suggest that HMB requires PPARα in upregulating morphological plasticity *in vivo* in the hippocampus of *5XFAD* mice.

Next, we explored the role of HMB in educating *5XFAD*$^{\Delta PPARα}$ mice in hippocampus-dependent behaviors including memory and learning. Although HMB treatment increased the performance of *5XFAD* mice on the Barnes maze (Figures 2L–2N) and T maze (Figures 2O–2P), this supplement could not protect spatial learning and memory in *5XFAD*$^{\Delta PPARα}$ mice, as evidenced from the heatmap (Figure 5G), latency (Figure 5H), and error (Figure 5I) from the Barnes maze and positive turn (Figure 5J) and negative turn (Figure 5K) from the T maze. These results demonstrate that HMB improves memory and learning in *5XFAD* mice via PPARα.

Oral HMB lowers the plaque burden in the brain of 5XFAD mice

Since amyloid plaques play an important role in the disease process of AD and such pathology is widespread in *5XFAD* mice,[27,30–33] we also examined whether oral

administration of HMB was capable of decreasing the amyloid load in the hippocampus, the most affected brain region in AD, of *5XFAD* mice. Aβ peptides are the main component of the amyloid plaques, and both common isoforms $A\beta_{40}$ and $A\beta_{42}$ are recognized by 6E10 monoclonal antibodies (mAbs). DAB immunostaining with 6E10 mAbs showed a remarkable increase in the Aβ in the hippocampus and cortex of *5XFAD* mice compared with non-Tg mice (Figures 6A–6C). Quantification of plaques in the hippocampus (Figures 6D–6F) and cortex (Figures 6G–6I) also corroborated the increase in plaques in the brain of *5XFAD* mice compared with non-Tg mice. However, oral administration of HMB significantly decreased the level of Aβ in the hippocampus and cortex of *5XFAD* mice (Figures 6A–6I). Immunoblot analysis of hippocampal homogenates with 6E10 mAbs also demonstrated a markedly higher level of Aβ peptides in the CNS of *5XFAD* mice compared with non-Tg mice (Figures 6J and 6K). However, similar to DAB staining, treatment of *5XFAD* mice with HMB led to a significant decrease in Aβ (Figures 6J and 6K).

To further confirm the deposition of amyloid plaques in the brain, we performed double labeling of hippocampal sections with thioflavin-S (thio-S), a classic amyloid-binding dye for the detection of the β-pleated sheet of the amyloid plaques, and 6E10. Consistent with the DAB and western blot results, a marked abundance of thio-S-positive and Aβ-immunoreactive plaques were observed in the CNS of *5XFAD* mice (Figures 7A and S9A). However, treatment of *5XFAD* mice with HMB decreased the plaque load (Figure 7A). Quantitative analysis of thio-S staining also showed that HMB treatment led to a significant decline in thio-S-positive area (Figure 7B), thio-S puncta (Figure 7C), and thio-S puncta size (Figure 7D) in the hippocampus of *5XFAD* mice. Moreover, ELISAs indicated an increase in Aβ1–42 (Figure 7E) and Aβ1–40 (Figure 7F) in serum of *5XFAD* mice compared with non-Tg mice. ELISAs of TBS-extracted (Figures S9B and S9C) and (TBS+Triton X-100)-extracted (Figures S9D and S9E) hippocampal extracts also showed upregulation of Aβ1–40 (Figures S9B and S9D) and Aβ1–42 (Figures S9C and S9E) in *5XFAD* mice compared with non-Tg mice. However, consistent with the decrease in amyloid pathology in the CNS, HMB treatment decreased the level of both Aβ1–42 (Figures 7E, S9C, and S9E) and Aβ1–40 (Figures 7F, S9B, and S9D) in serum (Figures 7E and 7F) and the hippocampus (Figures S9B–S9E) of *5XFAD* mice.

Oral administration of HMB reduces plaques from the hippocampus of 5XFAD mice via PPARα

Since HMB protects memory and learning in *5XFAD* mice via PPARα, next, we examined whether HMB also required PPARα to lower plaques from the hippocampus of *5XFAD* mice. Although HMB treatment decreased plaques from the brain of *5XFAD* mice (Figure 6), this supplement remained unable to reduce amyloid plaques from the hippocampus and cortex of $5XFAD^{\Delta PPARα}$ mice as is evident from DAB immunostaining of hippocampal and cortical sections of $5XFAD^{\Delta PPARα}$ mice (Figures S10A–S10C). Quantification of plaques in the hippocampus (Figures S10D–S10F) and cortex (Figures S10G–S10I) also showed that HMB treatment remained unable to decrease the number (Figures S10D and S10G), area (Figures S10E and S10H), and density (Figures S10F and S1I) of plaques in $5XFAD^{\Delta PPARα}$ mice. These results were also corroborated by western blot analysis of hippocampal extracts (Figures S10J–S10K). Thio-S and 6E10 double labeling also showed that HMB could

not inhibit the level of amyloid plaques (Figures 7A and S9A), decrease thio-S area (Figure 7B), reduce thio-S puncta (Figure 7C), or lower thio-S puncta size (Figure 7D) in the hippocampus of *5XFAD*$^{\Delta PPARα}$ mice. Consequently, HMB treatment also could not decrease Aβ1–42 (Figures 7E, S9C, and S9E) or Aβ1–40 (Figures 7F, S9B, and S9D) in serum (Figures 7E and 7F) and the hippocampus (Figures S9B–S9E) of *5XFAD*$^{\Delta PPARα}$ mice. Together, these results also suggest that HMB is unable to decrease plaques from the brain of *5XFAD* mice in the absence of PPARα.

DISCUSSION

At present, no effective treatment is available to prevent or halt the progression of AD. Therefore, describing non-toxic molecules for refining hippocampal functions, halting cognitive decline (the central clinical symptom of AD), and lowering senile plaques (one of the pathological markers of AD) is an important area of research. HMB is a widely used body-building supplement among muscle builders and combat sports athletes.[34] Here, we describe that oral HMB is capable of improving hippocampal plasticity, restoring cognitive functions, and reducing plaque load in *5XFAD* mouse models of AD. Since HMB is a non-toxic and easily available supplement, these results suggest that oral HMB may be used as a therapeutic supplement in patients with AD and MCI.

The hippocampus is endowed with unique functions of processing, organizing, and storing memories.[26,35] Therefore, upregulation of hippocampal plasticity is an important area of research for better therapeutic outcome in patients with AD. CREB is considered the master regulator of memory and learning, as almost all molecules, including BDNF, involved in hippocampal plasticity are transcriptionally controlled by CREB.[36–38] On the other hand, PPARα is a lipid-lowering transcription factor that, being abundant in the liver, helps in the reduction of triglycerides and free fatty acids via stimulation of peroxisomal β-oxidation of very-long-chain fatty acids.[6,7,39] Recently, we have seen that PPARα is also present in different regions of the brain including the hippocampus.[10,11,26] Interestingly, earlier, we demonstrated that the level of CREB is lower in the hippocampus of *PPARα*$^{-/-}$ mice, that CREB is transcriptionally regulated by PPARα, and that activation of PPARα stimulates hippocampal plasticity via an increase in CREB.[10] Moreover, upregulation of CREB and rebuilding of spatial learning and memory in *PPARα*$^{-/-}$ mice by lentiviral transfer of PPARα into the hippocampus proposes an important role of PPARα in cognitive functions.[10] Here, we have also seen that HMB treatment increases the level of CREB and CREB-associated plasticity-related molecules in the hippocampus, stimulates calcium oscillation in hippocampal slices, and improves spatial learning and memory in *5XFAD*, but not *5XFAD*$^{\Delta PPARα}$, mice. These results suggest that oral HMB is capable of upregulating CREB and improving CREB-dependent hippocampal functions in *5XFAD* mice via PPARα.

Many strategies for the development of novel therapeutics for AD have been focused on targeting the senile plaques that are formed by abnormal deposition of Aβ.[40] Senile plaques are broadly classified into two categories, such as diffuse and dense-core plaques. Diffuse plaques are thio-S negative, non-neuritic, and frequently observed in aged people who are cognitively intact. On the other hand, dense-core plaques that are present in the brains of patients with clinically identified AD stain positively for thio-S and are composed of

fibrillar Aβ. Mechanisms by which cerebral plaque level could be reduced are poorly understood. While the upregulation of the ADAM10-mediated nonamyloidogenic pathway inhibits the formation of amyloid plaques in neurons,[41] stimulation of the TFEB-driven lysosome-autophagy pathway increases the degradation of amyloid plaques.[42] On one hand, activation of PPARα stimulates the nonamyloidogenic pathway via transcriptional upregulation of ADAM10.[29] On the other, activated PPARα also leads to an increase in lysosomal biogenesis and autophagy via transcriptional stimulation of TFEB.[43,44] It has been demonstrated that PPARα, but neither PPARβ nor PPARγ, is directly recruited to the promoters of *ADAM10*[29] and *TFEB*[44] genes in response to gemfibrozil treatment. Therefore, PPARα plays a central role in controlling the level of plaques in the brain. Astrocytes are the major cell type in the brain, and recently, we also described that activation of PPARα is capable of enhancing astroglial uptake and degradation of Aβ.[32] It is important to mention that HMB is also capable of activating PPARα in primary astrocytes via interaction with the Y314 residue of PPARα (Figures 3H and 3I). Our current finding of lowering amyloid plaques by HMB treatment in *5XFAD*, but not *5XFAD*$^{\Delta PPARα}$ (*5XFAD* mice lacking PPARα), mice suggests that, similar to the improvement in cognitive functions, HMB treatment lowers plaque load in *5XFAD* mice via PPARα.

How does HMB involve PPARα to exhibit its memory-boosting and plaque-lowering activities? It is not known whether HMB is a ligand of PPARα. However, in cultured cells, HMB induces the activation of PPARα, as evidenced by increased nuclear translocation. The LBD of PPARα is quite large, with a 1,400-Å-wide pocket size that allows lipophilic compounds such as medium- and long-chain fatty acids to be docked inside.[45] However, a small polar environment is also maintained within the PPARα LBD by a catalytic triad of Ser280, Tyr314, and His440 to ultimately allow small polar compounds to be docked inside. It is believed that these three key residues stabilize the docking of partially polar compounds via the formation of H-bonds.[45] HMB is a negatively charged polar compound, and according to our *in silico* analysis, it forms H-bonds with the catalytic triad of the PPARα LBD. Upon analysis of the interaction of HMB with PPARα by different biophysical approaches such as TR-FRET and protein TSA, we have also seen strong binding of HMB with the PPARα LBD. Accordingly, HMB failed to activate PPARα, could not enhance morphological plasticity of hippocampal neurons, and remained unable to stimulate AMPA- and NMDA-induced calcium influx in mutated (Y314D) PPARα-transduced *PPARα*$^{-/-}$ hippocampal neurons, underlining the functional significance of HMB's interaction with the Y314 residue of PPARα LBD.

HMB is a very safe supplement, and even after long-term use, it does not exhibit any side effects. For muscle building, HMB is recommended at a dose of 3 g per day per adult. However, this 3 g should not be taken in one serving but rather split into 3 servings throughout the day, making it around 1g per serving per adult. If our mouse dose of HMB (5 or 10 mg/kg body wt/day) is translated to human, HMB at a dose of 400 or 800 mg per adult per day may be beneficial to control AD-related symptoms and pathology. Therefore, the dose at which HMB may improve memory and learning and lower the plaque burden in patients with AD is much lower than the dose that is being used to support body building in humans. In a 12 week, randomized, double-blind, placebo-controlled crossover study among 42 highly trained combat sports athletes,[46] HMB treatment led to increase in fat-free

mass with simultaneous decrease in fat mass. HMB treatment also increased aerobic and anaerobic capacity among combat sports athletes. Therefore, oral HMB should not exhibit toxicity in patients with AD and MCI.

Myokines/hepatokines, peptides produced and released by muscle/liver, are known to mediate communication between muscle and other organs.[47] Recent studies have shown that these molecules may play a role in streptozotocin-induced neuronal damage.[48] Since HMB is a muscle-building drug, future studies may be directed at defining the mechanism behind muscle-to-brain crosstalk and whether myokines/hepatokines play a role in HMB-mediated neuroprotection. In summary, HMB, a commonly used body-building supplement in human, binds to the LBD of PPARα to stimulate CREB and promote hippocampal plasticity via PPARα. After oral administration, HMB stimulates hippocampal function, defends spatial learning and memory, and lowers cerebral plaque load in an animal model of AD via PPARα. Therefore, HMB supplement may be beneficial for AD as well as other cognitive disorders.

Limitations of the study

Here, we have described that oral HMB reduces plaques and improves cognitive functions in 5XFAD mouse models of AD. Being a muscle-building supplement, HMB is known to strengthen muscle, and this property of HMB may contribute to HMB-mediated improved performance on the Barnes maze and T maze. However, here, we do not know whether this classical muscle-building property of HMB has any role in improved maze performance of 5XFAD mice. Therefore, experiments may be planned in the future to address these issues.

STAR★METHODS

RESOURCE AVAILABILITY

Lead contact—Further information and requests for resources and reagents should be directed to and will be fulfilled by the lead contact, Kalipada Pahan (Kalipada_Pahan@rush.edu).

Materials availability—Plasmids and mouse lines generated in this study are available from the lead contact upon request with a completed Materials Transfer Agreement.

Data and code availability

- Raw blots have been deposited at Figshare and are publicly available as of the date of publication. The DOI is listed in the key resources table. All other data reported in this paper will be shared by the lead contact upon request.
- This paper does not report any original code.
- Any additional information required to reanalyze the data reported in this work paper is available from the lead contact upon request.

EXPERIMENTAL MODEL AND STUDY PARTICIPANT DETAILS

Animals—*PPARα*$^{-/-}$ mice, *5XFAD [(APPwFILon, PSEN1*M146L*L286V)6799Vas/J]* mice,[30] and *C57BL/6J* mice (inbred of *5XFAD* mice) were obtained from Jackson Laboratory, Bar Harbor, ME, USA. Unless otherwise indicated, PPARα$^{-/-}$ mice[51] were maintained as homozygous on the *C57BL/6J* background. *5XFAD*$^{\Delta PPARα}$ mice, developed earlier by us[29] were maintained transgenic for the *5XFAD* mutations and homozygous for the *PPARα*$^{-/-}$ allele through genotyping as described by us.[9,29,52] Seven-month-old *5XFAD* and *5XFAD*$^{\Delta PPARα}$ mice of both sexes were used for experiments. Animal maintenance and experiments were performed in accordance with the National Institutes of Health guidelines and were approved by the Institutional Animal Care and Use committee of the Rush University Medical Center (IACUC protocol # 20–007). Animals were housed in the state-of-the art animal care facility of the Cohn Research Building of the Rush University Medical Center. Daily veterinary care were provided to all animals by the Vivarium staff under the supervision of the attending veterinarian, Dr. Jeffrey P. Ostwald.

Isolation of mouse hippocampal neurons—Dissociated hippocampal neuronal cultures were prepared from fetuses (E18) of pregnant *PPARα*$^{-/-}$ mice and strain-matched C57BL/6J littermate mice using methods similar to those described earlier with few modifications.[10,11,16,53] Briefly, hippocampi from fetal pups were isolated as a thin slice of tissue near the cortical edge of the medial temporal lobe and placed together in the Dulbecco's Modified Eagle Medium/Nutrient Mixture F-12 (DMEM/F12) media supplemented with 10% heat-inactivated fetal bovine serum. Cells were dissociated by trituration and single cell suspension was plated in a poly-D-lysine pre-coated 6 wells plate containing complete DMEM/F12 media. After cell attachment (5 min after plating), the DMEM/F12 media was replaced with Neurobasal Medium supplemented with B27 supplements (Life Technologies). Next day, 10μM AraC was added to remove glial contamination in the neuronal culture. Experiments were done in (9–10)-day-old pure hippocampal neuronal cultures. Immediately before experimental treatment, the medium was replaced with Neurobasal Medium without B27 supplements.

Isolation of mouse primary astrocytes—Astrocytes were isolated from mixed glial cultures of 7-day-old mouse pups following the protocol of Guilian and Baker[54] as described by us earlier.[55,56] Briefly, cerebral tissues collected from 7-day-old mouse pups were homogenized with glass mortar, triturated, passed through mesh, trypsinized, centrifuged, and mixed glial cells plated in DMEM/F-12 containing 10% fetal bovine serum. On day 9, the mixed glial cultures were washed three times with DMEM/F-12 and subjected to a shake at 240 rpm for 2 h at 37°C on a rotary shaker to remove loosely attached microglia. Attached cells were cultured again in DMEM/F-12 containing 10% FBS. On day 11, cells were shaken again at 180 rpm for 18 h to remove any remaining microglia. The adherent cells were washed and seeded onto new plates for further studies. By immunofluorescence assay, these cells homogeneously expressed glial fibrillary acidic protein (GFAP), a marker of astrocytes.[57]

METHOD DETAILS

Treatment of mice with HMB—Mice were treated orally with different doses (5 or 10 mg/kg body weight/day) of HMB solubilized in 100 μL water via a gavage needle. Therefore, control mice also received 100 μL water via gavage.

Typically, any animal experiment[27,31,58] is justifeid with 99% confidence interval that generates p = 0.99 and (1-p) = (1–0.99) = 0.01; ε is the margin of error = 0.05. Based on these values, the resultant sample size is:

$$N = \frac{1,28^2 * 0.99\left(1 - 0.99\right)}{0.05^2} = \frac{1,28^2 * 0.99 * 0.01}{0.05^2} = \frac{0.016}{0.0025} = 6.48 - 6$$ Therefore, six mice (n = 6) were used in each group. We used mice from both sexes (equal distribution).

DNA constructs and lentiviral transductions—Generation of the pCMV6-AC-GFP lentiviral backbone expressing TurboGFP (*OriGene #PS100010*) and *FL-PPARα* or *Y314D-PPARα* was described before.[10,11] Briefly, mouse PPARα ORF in pCMV6-AC-GFP vector (cat # MG 227641) was purchased from Origene followed by mutation at Tyr314 with aspartate (Y314D) by site-directed mutagenesis. To generate pLenti6.3/V5-TOPO® constructs of *FL-PPARα* or *Y314D-PPARα*, each construct was amplified by PCR followed by TOPO cloning reaction using Invitrogen kit (K5315–20) with pLenti6.3/V5-TOPO vector. One-Shot Stbl3 competent cells were used for transformation and sequencing of the clones was performed at ACGT Inc. Next, lentivirus production was carried out in 293FT cells using ViraPower™ Packaging Mix and pLenti expression plasmid DNA containing either *FL-PPARα* or *Y314D-PPARα*. Viral particles were concentrated with lenti-concentrator solution and MOI was calculated. During experiments, 10–12 days *in vitro* (DIV) PPARα$^{-/-}$ hippocampal neurons were transduced with lentiviral particles at MOI 10 for 48 h at 37°C. Live GFP imaging was used to monitor viral integration.

Calcium influx assay in hippocampal neurons—Calcium influx assay was carried out as described earlier.[10,11,16] Briefly, cultured hippocampal neurons were loaded with Fluo4-fluorescence conjugated calcium buffer (*Invitrogen Molecular Probes, Cat# F10471, F10472, and F10473*) and incubated at 37°C for 30 min following manufacture's protocol. Then excitation and emission were recorded in a *Perkin–Elmer Victor X2 Luminescence* spectrometer in the presence of NMDA (50 μM) and AMPA (50 μM). The induction of calcium current through NMDA and AMPA receptors are known to be influenced by a passive or secondary activation of AMPA and NMDA receptors, respectively. Therefore, in order to nullify the secondary involvement of NMDA activation in AMPA current, we used 20 μM N20C, a specific blocker of NMDA receptor. Similarly to eliminate the passive involvement of AMPA receptor in NMDA activation, we also used 50 μM Naspm, a specific AMPA blocker. The recording was done with 300 repeats at 0.1 ms intervals.

Thermal shift assay (TSA)—TSA was performed in QuantStudio 3 real-time thermal cycler with thermal shift dye kit (*Thermo Fisher*), as described before.[11,28,59] Briefly, purified protein (0.5 μg–1 μg) was added to 18 μL of thermal shift buffer and 1–2 μL of dye for each reaction. Reaction was fixed in 96-well PCR plate in dark and then placed in the thermal cycler using the following two-stage program ([25°C for 2 min] 1 cycle; [27°C

for 15 s, 26°C for 1 min] 70 cycles; auto increment 1°C for both stages). The filter was set at ROX with no passive filter and no quencher filter.

Time-resolved fluorescence energy transfer (TR-FRET) analysis—Lanthascreen TR-FRET PPARα coactivator assay kit was used for TR-FRET assay as described earlier.[11,28] Briefly, HMB was added to GST-tagged recombinant PPARα LBD, terbium (Tb)-tagged anti GST antibody, and fluorescein (FL)-tagged PGC-1α as mentioned in the manufacturer's protocol. Plate was centrifuged, incubated in dark for 30 min, and then analyzed in a Perkin–Elmer Victor X5 Luminescence spectrometer. The excitation and emission were set at 340 nm and 540 nm, respectively.

Immunocytochemistry—Primary hippocampal neurons were washed three times with 1X PBS, fixed in 4% paraformaldehyde for 10 min or with chilled methanol overnight, washed again with 1X PBS and incubated first with primary antibodies (Table S1) followed by Cy2 or Cy5 conjugated secondary antibodies. After secondary antibody incubation, coverslips were rinsed in 1X PBS, mounted on slides in Fluoromount *(Sigma)* and imaged using an *Olympus BX41* fluorescent microscope equipped with a *Hamamatsu ORCA-03G* camera.

Golgi staining—It was performed using a commercially-available kit (FD Rapid Golgistain Kit; FD Neurotechnologies, Inc., Baltimore, MD). Briefly, the brains were cut into 200-μm-thick coronal sections using a vibratome followed by mounting onto 2% gelatin-coated slides and airdrying at room temperature in the dark overnight. Following the instructions, sections were developed and dehydrated, and coverslipped with Permount. Golgi-stained cells were pictured by light microscopy. For calculation of spine density, the number of spines visible along a traced segment of dendrite was divided by the length of the traced segment.

Measurement of spine density and size—The spine density and size were measured as mentioned earlier.[10,11,16,28] Briefly, E18 hippocampal neurons were double-labeled with MAP2 and Alexa 647 conjugated phalloidin. Only densely stained neurons were counted. The total length of each dendrite was measured at 400× magnification using an *Olympus BX-41* fluorescence microscope. The number of spines on the dendrites was counted under oil immersion. Only spines that protruded laterally from the shafts of the dendrites into the surrounding area of clear neuropil were considered. The spine density of a hippocampal neuron was calculated by dividing the total number of spines on a neuron by the total length of its dendrites, and was expressed as the number of spines/10 μm dendrite. The size of the dendritic spines was measured by calculating the ratio of mean fluorescent intensity (MFI) of the spine head and MFI of the dendritic shaft.

Western blot—It was performed as described before.[60–62] For whole cell and tissue lysates, samples were homogenized in RIPA buffer containing protease and phosphatase inhibitors *(Sigma)*, rotated end over end for 30 min at 4°C and centrifuged for 10 min at 15,000g. The supernatant was aliquotted and stored at −80°C until use. Protein concentrations were determined using a *NanoDrop 2000* (*Thermo Fisher*), and 20–30 μg sample was heat-denatured and resolved on 10% or 12% polyacrylamide-SDS

gels in MES buffer or 1X SDS running buffer. Proteins were transferred to 0.45μm nitrocellulose membranes under wet conditions. Membranes were blocked for 1 h with Li-Cor blocking buffer, incubated with primary antibodies (Table S1) overnight at 4°C under shaking conditions, washed, incubated with IR-dye labeled secondary antibodies at room temperature, washed and visualized with the *Odyssey Infrared Imaging System (Li-Cor)*. Blots were converted to binary, analyzed using ImageJ (NIH) and normalized to the loading control (β-actin).

ELISA for Aβ40 and Aβ42—Hippocampal tissues were homogenized in TBS, pelleted for 30 min × 150,000*g*. The pellet was resuspended in 3 volumes (wt/vol original tissue weight) of TBS+1% Triton X-100, pelleted for 30 min × 150,000*g* and the supernatant recovered and stored. After measuring protein concentration, samples were diluted prior to performing ELISA according to manufacturer's instruction (BioLegend, SIG-38956).

Immunohistochemistry (IHC)—It was performed as described before.[60,63] Briefly, mice were anesthetized and perfused with PBS (pH 7.4) and then with 4% (w/v) paraformaldehyde solution in PBS followed by dissection of the brain from each mouse for IHC.[64,65] Samples were incubated in PBS containing 0.05% Tween 20 (PBST) and 10% sucrose for 3 h and then 30% sucrose overnight at 4°C. Brain was then embedded in O.C.T (Tissue Tech) at −80°C, and processed for conventional cryosectioning. Frozen sections (30 μm) were treated with cold ethanol (−20°C) followed by two rinses in PBS, blocking with 3% BSA in PBST and double labeling with two antibodies (Table S1). After three washes with PBST, sections were further incubated with Cy2 or Cy5 conjugated secondary antibodies (Jackson ImmunoResearch Laboratories, Inc.). The samples were mounted and observed under the *Olympus BX41* fluorescent microscope equipped with a *Hamamatsu ORCA-03G* camera. During Thio-S staining, after washing and incubation with secondary antibodies for 1 h, free-floating sections were stained with 0.002% Thio-S (Sigma) made up in TBS for 8 min. Sections were washed twice in 50% EtOH for 1 min and twice in TBS for 5 min before drying and mounting in Fluoromount (Sigma).

Thio-S quantification—It was performed on two sections (one image per section) of each of six mice per group as described before.[29,52] First, grayscale images were uniformly thresholded and made binary with Fiji. Using the analyze particles function, Thio-S-positive area percentage, Thio-S puncta count, and Thio-S puncta size were determined.

Measurement of mean fluorescence intensity (MFI)—The "measurement module" of the microsuite V Olympus software was used to measure MFI as described before.[63,66] Briefly, images were opened in their respective channel followed by launching the measurement module and selection of two parameters including perimeter and MFI. The rectangular box tool was used to outline the perimeter and then associated MFI in that given perimeter was automatically calculated.

Organotypic calcium influx assay—Calcium influx was assayed in hippocampal slices as described before.[11,16] Briefly, mice were anesthetized, rapidly perfused with ice-cold sterile PBS, and decapitated. The whole brain was carefully removed from the cranium. Dorsoventral slices of the hippocampus were made at a thickness of 100 μm using adult

mouse brain slicer matrix with 1.0 mm coronal section slice intervals. The slices were placed in the glass tray filled with cutting solution (sucrose 24.56 g, dextrose 0.9008 g, ascorbate 0.0881 g, sodium pyruvate 0.1650 g, and myo-inositol 0.2703 g in 500 mL distilled water) that was continuously bubbled with 5% CO_2 and 95% O_2 gas mixture. The glass tray was kept ice-cold during the slicing period. Slices were then carefully transferred into Fluo-4 dye containing reaction buffer. The reaction buffer was made prior to the making of brain slices using 10 mL of artificial CSF (119 mM NaCl, 26.2 mM NaHCO3, 2.5 mM KCl, 1 mM NaH2PO4, 1.3 mM MgCl2, 10 mM glucose, bubbled with 5% CO2 and 95% O2 followed by the addition of 2.5 mM CaCl2) added to one bottle of Fluo-4 dye (Cat# F10471), and 250 mM probenecid. Before transferring slices, a flat bottom 96 well plate was loaded with 50 μL of reaction buffer per well, covered with aluminum foil, and kept in a dark place. One individual slice was placed in each well loaded with reaction buffer, and the plate was re-wrapped with aluminum foil and kept at 37°C for 20 min followed by recording excitation and emission in a *Perkin–Elmer Victor X2 Luminescence* spectrometer in the presence of NMDA (50 μM) and AMPA (50 μM). The recording was carried out with 300 repeats at 0.1 ms intervals.

Barnes maze and T maze—These experiments were performed as described before.[10,67] Briefly, for Barnes maze, mice were trained for 2 consecutive days followed by examination on day 3. During training, the overnight food-deprived mouse was placed in the middle of the maze in a 10 cm high cylindrical start chamber. After 10 s, the start chamber was removed to allow the mouse to move around the maze to find out the color food chips in the baited tunnel. The session was ended when the mouse entered the baited tunnel. On day 3, a video camera *(Basler Gen I Cam - Basler acA 1300–60)* connected to a *Noldus* computer system was placed above the maze and was illuminated with high wattage light that generated enough light and heat to motivate animals to enter into the escape tunnel. The performance was monitored by the EthoVision XT video tracking system *(Noldus)*. Cognitive parameters were analyzed by measuring latency (duration before all four paws were on the floor of the escape box) and errors (incorrect responses before all four paws were on the floor of the escape box).

For T-maze, mice were also habituated in the T-maze for two days under food-deprived conditions so that animals can eat food rewards at least five times during 10 min period of training. During each trial, mice were placed in the start point for 30 s and then forced to make a right arm turn which was always baited with color food chips. On entering the right arm, they were allowed to stay there for 30–45 s, then returned to the start point, held for 30 s and then allowed to make right turn again. After each training session, both Barnes maze and T-maze were thoroughly cleaned with a mild detergent. On day 3, mice were tested for making positive turns and negative turns. The reward side is always associated with a visual cue. The number of times the animal eats the food reward would be considered as a positive turn.

QUANTIFICATION AND STATISTICAL ANALYSIS

Results were statistically analyzed using GraphPad Prism version 9.5.1 (733). Values are expressed as either mean ± SD or mean ± SEM. Statistical comparisons between two

different samples were conducted by two-sample t test. On the other hand, one-way ANOVA followed by Tukey's multiple comparisons was performed for statistical analyses among multiple groups. For analyzing AMPA- and NMDA-induced calcium influx, repeated measure two-way ANOVA was performed followed by either Sidak's post hoc test or Tukey's post hoc test. The criterion for statistical significance was $p < 0.05$. Statistical details of experiments can be found under figure legends.

Supplementary Material

Refer to Web version on PubMed Central for supplementary material.

ACKNOWLEDGMENTS

This work was supported by grants (AT10980, AT10980-01S1, and AT10980-03S1) from NIH. Moreover, K.P. is the recipient of a Research Career Scientist Award (1IK6 BX004982) from the Department of Veterans Affairs. However, the views expressed in this article are those of the authors and do not necessarily reflect the position or policy of the Department of Veterans Affairs or the United States government.

REFERENCES

1. Reitz C, Brayne C, and Mayeux R (2011). Epidemiology of Alzheimerdisease. Nat. Rev. Neurol. 7, 137–152. 10.1038/nrneurol.2011.2. [PubMed: 21304480]
2. Hardy J, Duff K, Hardy KG, Perez-Tur J, and Hutton M (1998). Genetic dissection of Alzheimer's disease and related dementias: amyloid and its relationship to tau. Nat. Neurosci. 1, 355–358. 10.1038/1565. [PubMed: 10196523]
3. Tanzi RE, and Bertram L (2005). Twenty years of the Alzheimer's disease amyloid hypothesis: a genetic perspective. Cell 120, 545–555. 10.1016/j.cell.2005.02.008. [PubMed: 15734686]
4. Nussbaum RL, and Ellis CE (2003). Alzheimer's disease and Parkinson's disease. N. Engl. J. Med. 348, 1356–1364. 10.1056/NEJM2003ra020003. [PubMed: 12672864]
5. Scheff SW, Price DA, Schmitt FA, and Mufson EJ (2006). Hippocampal synaptic loss in early Alzheimer's disease and mild cognitive impairment. Neurobiol. Aging 27, 1372–1384. 10.1016/j.neurobiolaging.2005.09.012. [PubMed: 16289476]
6. Pahan K (2006). Lipid-lowering drugs. Cell. Mol. Life Sci. 63, 1165–1178. 10.1007/s00018-005-5406-7. [PubMed: 16568248]
7. Schoonjans K, Peinado-Onsurbe J, Lefebvre AM, Heyman RA, Briggs M, Deeb S, Staels B, and Auwerx J (1996). PPARαlpha and PPARgamma activators direct a distinct tissue-specific transcriptional response via a PPRE in the lipoprotein lipase gene. EMBO J. 15, 5336–5348. [PubMed: 8895578]
8. Patel D, Roy A, Kundu M, Jana M, Luan CH, Gonzalez FJ, and Pahan K (2018). Aspirin binds to PPARαlpha to stimulate hippocampal plasticity and protect memory. Proc. Natl. Acad. Sci. USA 115, E7408–E7417. 10.1073/pnas.1802021115. [PubMed: 30012602]
9. Patel D, Roy A, Raha S, Kundu M, Gonzalez FJ, and Pahan K (2020). Upregulation of BDNF and hippocampal functions by a hippocampal ligand of PPARαlpha. JCI Insight 5, e136654. 10.1172/jci.insight.136654. [PubMed: 32315292]
10. Roy A, Jana M, Corbett GT, Ramaswamy S, Kordower JH, Gonzalez FJ, and Pahan K (2013). Regulation of cyclic AMP response element binding and hippocampal plasticity-related genes by peroxisome proliferator-activated receptor alpha. Cell Rep. 4, 724–737. 10.1016/j.celrep.2013.07.028. [PubMed: 23972989]
11. Roy A, Jana M, Kundu M, Corbett GT, Rangaswamy SB, Mishra RK, Luan CH, Gonzalez FJ, and Pahan K (2015). HMG-CoA Reductase Inhibitors Bind to PPARαlpha to Upregulate Neurotrophin Expression in the Brain and Improve Memory in Mice. Cell Metab. 22, 253–265. 10.1016/j.cmet.2015.05.022. [PubMed: 26118928]

12. Counts SE, Alldred MJ, Che S, Ginsberg SD, and Mufson EJ (2014). Synaptic gene dysregulation within hippocampal CA1 pyramidal neurons in mild cognitive impairment. Neuropharmacology 79, 172–179. 10.1016/j.neuropharm.2013.10.018. [PubMed: 24445080]

13. Mufson EJ, Mahady L, Waters D, Counts SE, Perez SE, DeKosky ST, Ginsberg SD, Ikonomovic MD, Scheff SW, and Binder LI (2015). Hippocampal plasticity during the progression of Alzheimer's disease. Neuroscience 309, 51–67. 10.1016/j.neuroscience.2015.03.006. [PubMed: 25772787]

14. Skaper SD, Facci L, Zusso M, and Giusti P (2017). Synaptic Plasticity, Dementia and Alzheimer Disease. CNS Neurol. Disord.: Drug Targets 16, 220–233. 10.2174/1871527316666170113120853.

15. Ultanir SK, Kim JE, Hall BJ, Deerinck T, Ellisman M, and Ghosh A (2007). Regulation of spine morphology and spine density by NMDA receptor signaling *in vivo*. Proc. Natl. Acad. Sci. USA 104, 19553–19558. 10.1073/pnas.0704031104. [PubMed: 18048342]

16. Roy A, Modi KK, Khasnavis S, Ghosh S, Watson R, and Pahan K (2014). Enhancement of morphological plasticity in hippocampal neurons by a physically modified saline via phosphatidylinositol-3 kinase. PLoS One 9, e101883. 10.1371/journal.pone.0101883. [PubMed: 25007337]

17. Sakimura K, Kutsuwada T, Ito I, Manabe T, Takayama C, Kushiya E, Yagi T, Aizawa S, Inoue Y, Sugiyama H, et al. (1995). Reduced hippocampal LTP and spatial learning in mice lacking NMDA receptor epsilon 1 subunit. Nature 373, 151–155. 10.1038/373151a0. [PubMed: 7816096]

18. Lee HK, Takamiya K, Han JS, Man H, Kim CH, Rumbaugh G, Yu S, Ding L, He C, Petralia RS, et al. (2003). Phosphorylation of the AMPA receptor GluR1 subunit is required for synaptic plasticity and retention of spatial memory. Cell 112, 631–643. 10.1016/s0092-8674(03)00122-3. [PubMed: 12628184]

19. Kennedy MB, Beale HC, Carlisle HJ, and Washburn LR (2005). Integration of biochemical signalling in spines. Nat. Rev. Neurosci. 6, 423–434. 10.1038/nrn1685. [PubMed: 15928715]

20. Tada T, and Sheng M (2006). Molecular mechanisms of dendritic spine morphogenesis. Curr. Opin. Neurobiol. 16, 95–101. 10.1016/j.conb.2005.12.001.. [PubMed: 16361095]

21. Alvarez VA, and Sabatini BL (2007). Anatomical and physiological plasticity of dendritic spines. Annu. Rev. Neurosci. 30, 79–97. 10.1146/annurev.neuro.30.051606.094222. [PubMed: 17280523]

22. VanGuilder HD, Farley JA, Yan H, Van Kirk CA, Mitschelen M, Sonntag WE, and Freeman WM (2011). Hippocampal dysregulation of synaptic plasticity-associated proteins with age-related cognitive decline. Neurobiol. Dis. 43, 201–212. 10.1016/j.nbd.2011.03.012. [PubMed: 21440628]

23. Brinkmalm A, Brinkmalm G, Honer WG, Frölich L, Hausner L, Minthon L, Hansson O, Wallin A, Zetterberg H, Blennow K, and Öhrfelt A (2014). SNAP-25 is a promising novel cerebrospinal fluid biomarker for synapse degeneration in Alzheimer's disease. Mol. Neurodegener. 9, 53. 10.1186/1750-1326-9-53. [PubMed: 25418885]

24. Lipsky RH, and Marini AM (2007). Brain-derived neurotrophic factor in neuronal survival and behavior-related plasticity. Ann. N. Y. Acad. Sci. 1122, 130–143. 10.1196/annals.1403.009. [PubMed: 18077569]

25. Kellner Y, Gödecke N, Dierkes T, Thieme N, Zagrebelsky M, and Korte M (2014). The BDNF effects on dendritic spines of mature hippocampal neurons depend on neuronal activity. Front. Synaptic Neurosci. 6, 5. 10.3389/fnsyn.2014.00005. [PubMed: 24688467]

26. Roy A, and Pahan K (2015). PPARαlpha signaling in the hippocampus: crosstalk between fat and memory. J. Neuroimmune Pharmacol. 10, 30–34. 10.1007/s11481-014-9582-9. [PubMed: 25575492]

27. Rangasamy SB, Corbett GT, Roy A, Modi KK, Bennett DA, Mufson EJ, Ghosh S, and Pahan K (2015). Intranasal Delivery of NEMO-Binding Domain Peptide Prevents Memory Loss in a Mouse Model of Alzheimer's Disease. J. Alzheimers Dis. 47, 385–402. 10.3233/JAD-150040. [PubMed: 26401561]

28. Roy A, Kundu M, Jana M, Mishra RK, Yung Y, Luan CH, Gonzalez FJ, and Pahan K (2016). Identification and characterization of PPARαlpha ligands in the hippocampus. Nat. Chem. Biol. 12, 1075–1083. 10.1038/nchembio.2204. [PubMed: 27748752]

29. Corbett GT, Gonzalez FJ, and Pahan K (2015). Activation of peroxisome proliferator-activated receptor alpha stimulates ADAM10-mediated proteolysis of APP. Proc. Natl. Acad. Sci. USA 112, 8445–8450. 10.1073/pnas.1504890112. [PubMed: 26080426]
30. Oakley H, Cole SL, Logan S, Maus E, Shao P, Craft J, Guillozet-Bongaarts A, Ohno M, Disterhoft J, Van Eldik L, et al. (2006). Intra-neuronal beta-amyloid aggregates, neurodegeneration, and neuron loss in transgenic mice with five familial Alzheimer's disease mutations: potential factors in amyloid plaque formation. J. Neurosci. 26, 10129–10140. 10.1523/JNEUROSCI.1202-06.2006. [PubMed: 17021169]
31. Modi KK, Roy A, Brahmachari S, Rangasamy SB, and Pahan K (2015). Cinnamon and Its Metabolite Sodium Benzoate Attenuate the Activation of p21rac and Protect Memory and Learning in an Animal Model of Alzheimer's Disease. PLoS One 10, e0130398. 10.1371/journal.pone.0130398. [PubMed: 26102198]
32. Raha S, Ghosh A, Dutta D, Patel DR, and Pahan K (2021). Activation of PPARαlpha enhances astroglial uptake and degradation of beta-amyloid. Sci. Signal. 14, eabg4747. 10.1126/scisignal.abg4747. [PubMed: 34699252]
33. Rangasamy SB, Jana M, Roy A, Corbett GT, Kundu M, Chandra S, Mondal S, Dasarathi S, Mufson EJ, Mishra RK, et al. (2018). Selective disruption of TLR2-MyD88 interaction inhibits inflammation and attenuates Alzheimer's pathology. J. Clin. Invest. 128, 4297–4312. 10.1172/JCI96209. [PubMed: 29990310]
34. Lin Z, Zhao A, and He J (2022). Effect of beta-hydroxy-beta-methylbutyrate (HMB) on the Muscle Strength in the Elderly Population: A Meta-Analysis. Front. Nutr. 9, 914866. 10.3389/fnut.2022.914866.
35. Eichenbaum H (2017). Memory: Organization and Control. Annu. Rev. Psychol. 68, 19–45. 10.1146/annurev-psych-010416-044131. [PubMed: 27687117]
36. Frank DA, and Greenberg ME (1994). CREB: a mediator of long-term memory from mollusks to mammals. Cell 79, 5–8. 10.1016/0092-8674(94)90394-8. [PubMed: 7923377]
37. Hong EJ, West AE, and Greenberg ME (2005). Transcriptional control of cognitive development. Curr. Opin. Neurobiol. 15, 21–28. 10.1016/j.conb.2005.01.002. [PubMed: 15721740]
38. Ghosh A, Ginty DD, Bading H, and Greenberg ME (1994). Calcium regulation of gene expression in neuronal cells. J. Neurobiol. 25, 294–303. 10.1002/neu.480250309. [PubMed: 7910846]
39. Marcus SL, Miyata KS, Zhang B, Subramani S, Rachubinski RA, and Capone JP (1993). Diverse peroxisome proliferator-activated receptors bind to the peroxisome proliferator-responsive elements of the rat hydratase/dehydrogenase and fatty acyl-CoA oxidase genes but differentially induce expression. Proc. Natl. Acad. Sci. USA 90, 5723–5727. 10.1073/pnas.90.12.5723. [PubMed: 8390676]
40. LaFerla FM, Green KN, and Oddo S (2007). Intracellular amyloid-beta in Alzheimer's disease. Nat. Rev. Neurosci. 8, 499–509. 10.1038/nrn2168. [PubMed: 17551515]
41. Lichtenthaler SF, Tschirner SK, and Steiner H (2022). Secretases in Alzheimer's disease: Novel insights into proteolysis of APP and TREM2. Curr. Opin. Neurobiol. 72, 101–110. 10.1016/j.conb.2021.09.003. [PubMed: 34689040]
42. Gu Z, Cao H, Zuo C, Huang Y, Miao J, Song Y, Yang Y, Zhu L, and Wang F (2022). TFEB in Alzheimer's disease: From molecular mechanisms to therapeutic implications. Neurobiol. Dis. 173, 105855. 10.1016/j.nbd.2022.105855. [PubMed: 36031168]
43. Ghosh A, and Pahan K (2016). PPARαlpha in lysosomal biogenesis: A perspective. Pharmacol. Res. 103, 144–148. 10.1016/j.phrs.2015.11.011. [PubMed: 26621249]
44. Ghosh A, Jana M, Modi K, Gonzalez FJ, Sims KB, Berry-Kravis E, and Pahan K (2015). Activation of peroxisome proliferator-activated receptor alpha induces lysosomal biogenesis in brain cells: implications for lysosomal storage disorders. J. Biol. Chem. 290, 10309–10324. 10.1074/jbc.M114.610659. [PubMed: 25750174]
45. Xu HE, Lambert MH, Montana VG, Plunket KD, Moore LB, Collins JL, Oplinger JA, Kliewer SA, Gampe RT Jr., McKee DD, et al. (2001). Structural determinants of ligand binding selectivity between the peroxisome proliferator-activated receptors. Proc. Natl. Acad. Sci. USA 98, 13919–13924. 10.1073/pnas.241410198. [PubMed: 11698662]

46. Durkalec-Michalski K, Jeszka J, and Podgórski T (2017). The Effect of a 12-Week Beta-hydroxy-beta-methylbutyrate (HMB) Supplementation on Highly-Trained Combat Sports Athletes: A Randomised, DoubleBlind, Placebo-Controlled Crossover Study. Nutrients 9, 753. 10.3390/nu9070753. [PubMed: 28708126]
47. Chung HS, and Choi KM (2020). Organokines in disease. Adv. Clin. Chem. 94, 261–321. 10.1016/bs.acc.2019.07.012. [PubMed: 31952573]
48. Lee H, and Lim Y (2022). The Potential Role of Myokines/Hepatokines in the Progression of Neuronal Damage in Streptozotocin and High-Fat Diet-Induced Type 2 Diabetes Mellitus Mice. Biomedicines 10, 1521. 10.3390/biomedicines10071521. [PubMed: 35884825]
49. Jana M, Mondal S, Gonzalez FJ, and Pahan K (2012). Gemfibrozil, a lipid-lowering drug, increases myelin genes in human oligodendrocytes via peroxisome proliferator-activated receptor-beta. J. Biol. Chem. 287, 34134–34148. 10.1074/jbc.M112.398552. [PubMed: 22879602]
50. Schneider CA, Rasband WS, and Eliceiri KW (2012). NIH Image to ImageJ: 25 years of image analysis. Nat. Methods 9, 671–675. 10.1038/nmeth.2089. [PubMed: 22930834]
51. Peters JM, Lee SS, Li W, Ward JM, Gavrilova O, Everett C, Reitman ML, Hudson LD, and Gonzalez FJ (2000). Growth, adipose, brain, and skin alterations resulting from targeted disruption of the mouse peroxisome proliferator-activated receptor beta(delta). Mol. Cell Biol. 20, 5119–5128. [PubMed: 10866668]
52. Chandra S, Jana M, and Pahan K (2018). Aspirin Induces Lysosomal Biogenesis and Attenuates Amyloid Plaque Pathology in a Mouse Model of Alzheimer's Disease via PPARαlpha. J. Neurosci. 38, 6682–6699. 10.1523/JNEUROSCI.0054-18.2018. [PubMed: 29967008]
53. Jana M, Jana A, Pal U, and Pahan K (2007). A simplified method for isolating highly purified neurons, oligodendrocytes, astrocytes, and microglia from the same human fetal brain tissue. Neurochem. Res. 32, 2015–2022. 10.1007/s11064-007-9340-y. [PubMed: 17447141]
54. Giulian D, and Baker TJ (1986). Characterization of ameboid microglia isolated from developing mammalian brain. J. Neurosci. 6, 2163–2178. [PubMed: 3018187]
55. Dasgupta S, Jana M, Liu X, and Pahan K (2003). Role of very-late antigen-4 (VLA-4) in myelin basic protein-primed T cell contact-induced expression of proinflammatory cytokines in microglial cells. J. Biol. Chem. 278, 22424–22431. [PubMed: 12690109]
56. Roy A, Fung YK, Liu X, and Pahan K (2006). Up-regulation of microglial CD11b expression by nitric oxide. J. Biol. Chem. 281, 14971–14980. 10.1074/jbc.M600236200. [PubMed: 16551637]
57. Brahmachari S, Fung YK, and Pahan K (2006). Induction of glial fibrillary acidic protein expression in astrocytes by nitric oxide. J. Neurosci. 26, 4930–4939. [PubMed: 16672668]
58. Modi KK, Jana A, Ghosh S, Watson R, and Pahan K (2014). A physically-modified saline suppresses neuronal apoptosis, attenuates tau phosphorylation and protects memory in an animal model of Alzheimer's disease. PLoS One 9, e103606. 10.1371/journal.pone.0103606. [PubMed: 25089827]
59. Paidi RK, Jana M, Raha S, McKay M, Sheinin M, Mishra RK, and Pahan K (2021). Eugenol, a Component of Holy Basil (Tulsi) and Common Spice Clove, Inhibits the Interaction Between SARS-CoV-2 Spike S1 and ACE2 to Induce Therapeutic Responses. J. Neuroimmune Pharmacol. 16, 743–755. 10.1007/s11481-021-10028-1. [PubMed: 34677731]
60. Dutta D, Jana M, Majumder M, Mondal S, Roy A, and Pahan K (2021). Selective targeting of the TLR2/MyD88/NF-kappaB pathway reduces alpha-synuclein spreading in vitro and *in vivo*. Nat. Commun. 12, 5382. 10.1038/s41467-021-25767-1. [PubMed: 34508096]
61. Paidi RK, Jana M, Mishra RK, Dutta D, and Pahan K (2021). Selective Inhibition of the Interaction between SARS-CoV-2 Spike S1 and ACE2 by SPIDAR Peptide Induces Anti-Inflammatory Therapeutic Responses. J. Immunol. 207, 2521–2533. 10.4049/jimmunol.2100144. [PubMed: 34645689]
62. Mondal S, Kundu M, Jana M, Roy A, Rangasamy SB, Modi KK, Wallace J, Albalawi YA, Balabanov R, and Pahan K (2020). IL-12 p40 monomer is different from other IL-12 family members to selectively inhibit IL-12Rbeta1 internalization and suppress EAE. Proc. Natl. Acad. Sci. USA 117, 21557–21567. 10.1073/pnas.2000653117. [PubMed: 32817415]

63. Dutta D, Paidi RK, Raha S, Roy A, Chandra S, and Pahan K (2022). Treadmill exercise reduces alpha-synuclein spreading via PPARαlpha. Cell Rep. 40, 111058. 10.1016/j.celrep.2022.111058. [PubMed: 35830804]

64. Khasnavis S, Roy A, Ghosh S, Watson R, and Pahan K (2014). Protection of dopaminergic neurons in a mouse model of Parkinson's disease by a physically-modified saline containing charge-stabilized nanobubbles. J. Neuroimmune Pharmacol. 9, 218–232. 10.1007/s11481-013-9503-3. [PubMed: 24122363]

65. Ghosh A, Roy A, Liu X, Kordower JH, Mufson EJ, Hartley DM, Ghosh S, Mosley RL, Gendelman HE, and Pahan K (2007). Selective inhibition of NF-kappaB activation prevents dopaminergic neuronal loss in a mouse model of Parkinson's disease. Proc. Natl. Acad. Sci. USA 104, 18754–18759. [PubMed: 18000063]

66. Chandra G, Roy A, Rangasamy SB, and Pahan K (2017). Induction of Adaptive Immunity Leads to Nigrostriatal Disease Progression in MPTP Mouse Model of Parkinson's Disease. J. Immunol. 198, 4312–4326. 10.4049/jimmunol.1700149. [PubMed: 28446566]

67. Corbett GT, Roy A, and Pahan K (2013). Sodium phenylbutyrate enhances astrocytic neurotrophin synthesis via protein kinase C (PKC)-mediated activation of cAMP-response element-binding protein (CREB): implications for Alzheimer disease therapy. J. Biol. Chem. 288, 8299–8312. 10.1074/jbc.M112.426536. [PubMed: 23404502]

Highlights

- Muscle-building supplement HMB binds to PPARα
- HMB increases morphological plasticity of hippocampal neurons via PPARα
- Oral HMB improves hippocampal functions in 5XFAD mice using PPARα
- Oral HMB lowers plaques in 5XFAD mice through PPARα

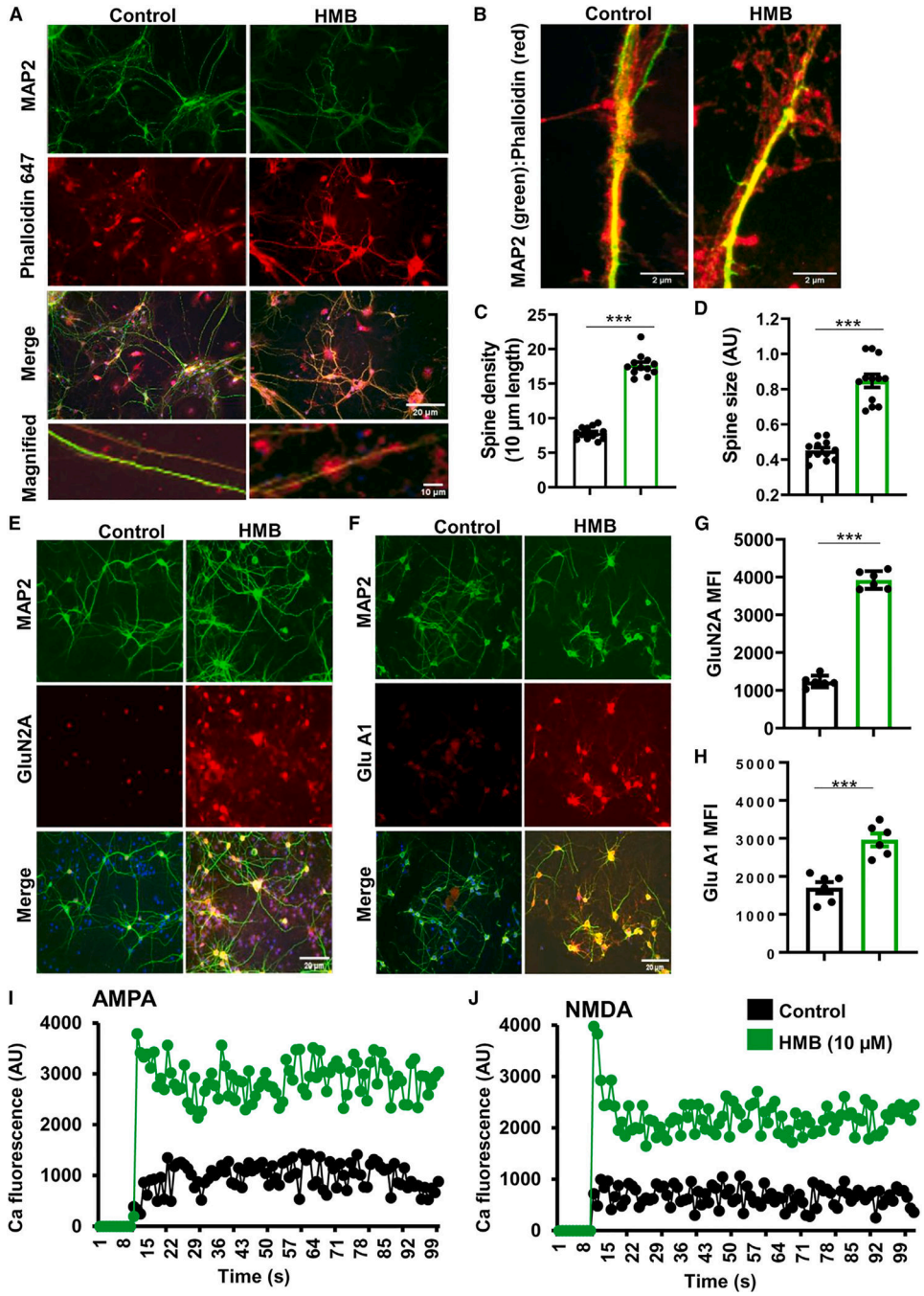

Figure 1. HMB upregulates morphological plasticity in hippocampal neurons

(A) Hippocampal neurons were treated with 10 μM HMB for 24 h followed by double labeling with neuronal marker MAP2 (green) and Alexa 647-conjugated phalloidin (red) for spines.

(B–D) Images were magnified (B) to monitor spine morphology (C, spine density; D, spine size) from a total of 13 different neurons from three different experiments. ***$p < 0.001$.

(E–H) After treatment with HMB, hippocampal neurons were double labeled with either MAP2 and NR2A (E) or MAP2 and GluR1 (F) followed by quantification of mean

fluorescence intensity (MFI) of NR2A (G) and GluR1 (H) in six images per group from a total of three independent experiments using NIH ImageJ. Results were analyzed by two-sample t test. ***$p < 0.001$.

(I and J) AMPA- (I) and NMDA-induced (J) calcium influx was monitored in a PerkinElmer Victor X2 luminescence spectrometer. To nullify the secondary involvement of AMPA receptor in NMDA-dependent calcium currents, hippocampal neurons were treated with NMDA together with Naspm followed by the recording of calcium influx. Similarly, AMPA-dependent calcium influx was measured in the presence of N20C. Results are presented as the mean of three independent experiments. Results were statistically analyzed by repeated measure two-way ANOVA followed by Sidak's post hoc test. $p < 0.05$ (= 0.0154) control vs. HMB for AMPA; $p < 0.05$ (= 0.0157) control vs. HMB for NMDA.

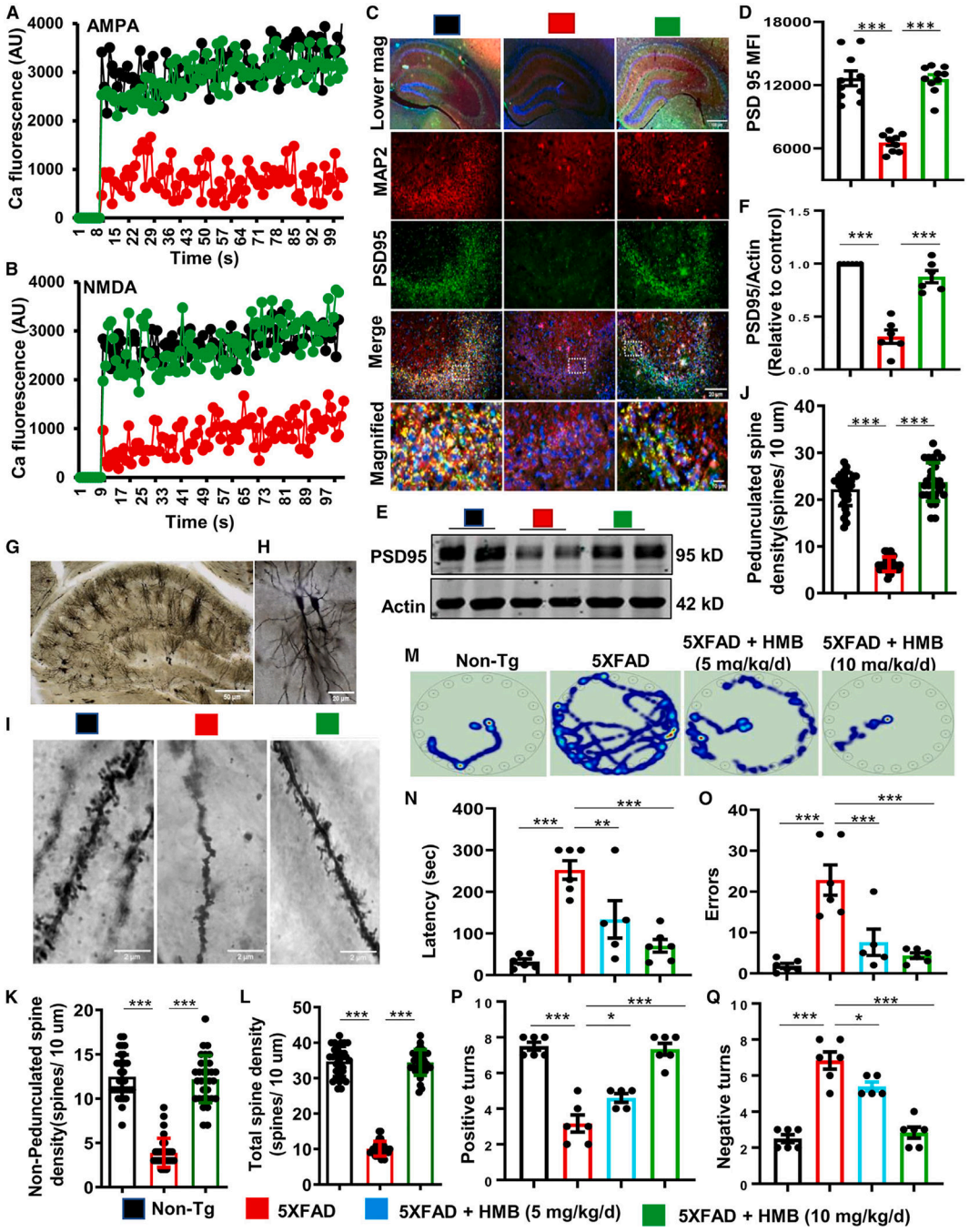

Figure 2. Oral administration of HMB promotes calcium influx in the hippocampus and improves spatial learning and memory of *5XFAD* mice

Seven-month-old *5XFAD* mice (n = 6 per group) were treated with HMB (10 mg/kg body wt/day) via gavage once daily. Since HMB was solubilized in 100 μL water, control *5XFAD* mice also received the same volume of water as vehicle via gavage.

(A and B) After 30 days of treatment, (A) AMPA- and (B) NMDA-dependent calcium currents were measured in the hippocampal slices of different groups of mice. Results were statistically analyzed by repeated measure two-way ANOVA followed by Tukey's post hoc

test. $p < 0.001$ (= 0.0005) 5XFAD vs. 5XFAD+HMB for AMPA; $p < 0.01$ (= 0.0017) 5XFAD vs. 5XFAD+HMB for NMDA.

(C and D) Hippocampal sections were double labeled for MAP2 and PSD95 (C) followed by quantification of PSD95 MFI on 10 images from a total of 6 mice per group (D).

(E and F) Hippocampal extracts were immunoblotted for PSD95 (E). Bands were scanned and values (PSD95/actin) (F) presented as relative to control. Values are mean ± SEM of six mice per group. Golgi staining was performed on hippocampal sections.

(G and H) Image of the hippocampus (G) and microphotograph of a CA1 pyramidal neuron (H).

(I) Dendritic spines in the apical dendrites of hippocampal CA1 pyramidal neurons are shown for different groups.

(J–L) Bar graphs show number of pedunculated spines (J), non-pedunculated spines (K), and total spines (L) per 10 μm apical dendrites.

(M–Q) After 30 days of treatment with different doses of HMB, mice were tested for Barnes maze (M, heatmap; N, latency; O, error) and T maze (P, positive turn; Q, negative turn). Results are mean ± SEM of six mice per group. One-way ANOVA followed by Tukey's multiple comparison test were used for statistical analysis.

***$p < 0.001$; **$p < 0.01$; *$p < 0.05$.

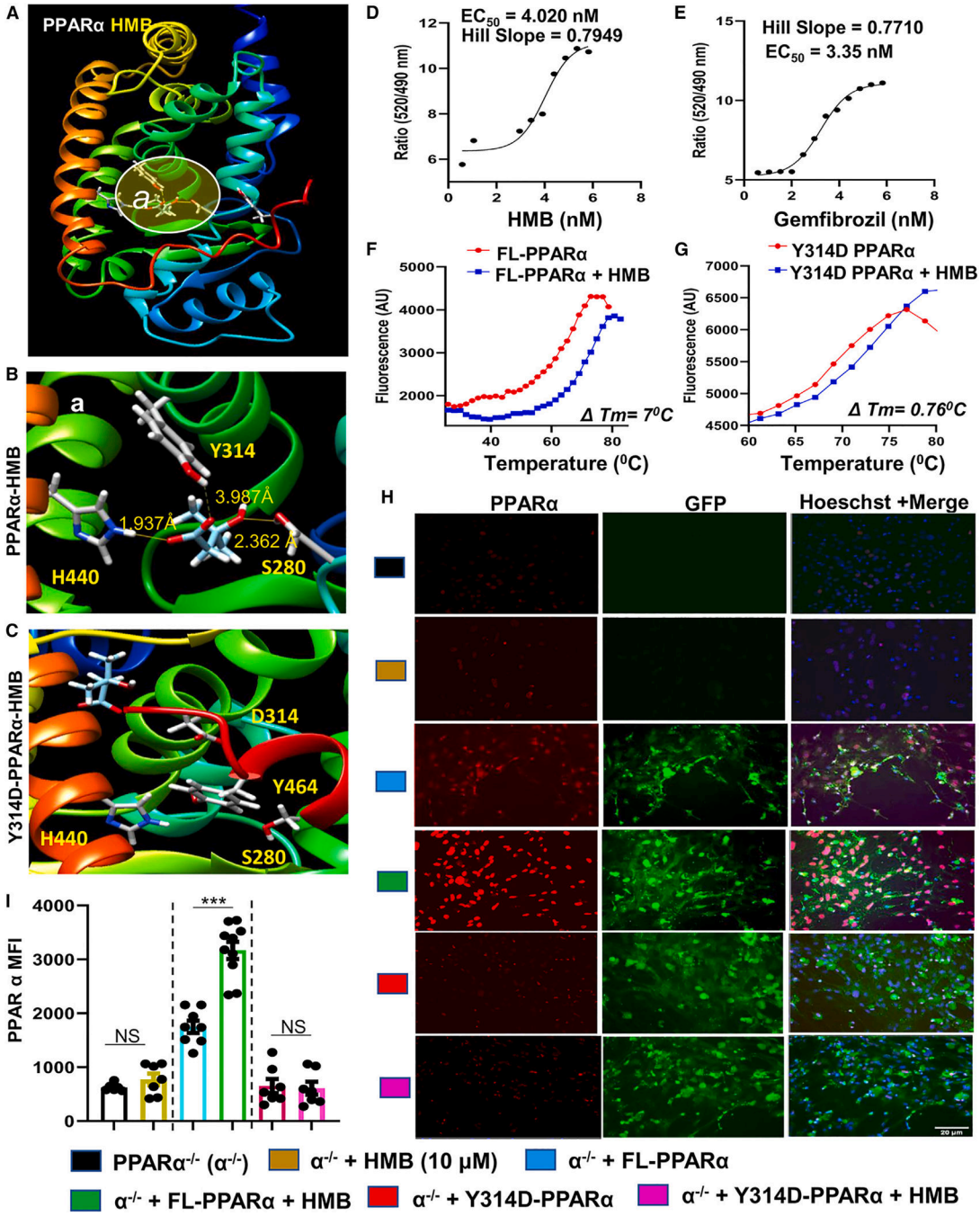

Figure 3. Characterization of interaction of HMB with PPARα at *in silico* and molecular levels

(A) A rigid body *in silico* docked pose of the PPARα LBD with HMB was derived from the SwissDock online server and then displayed in UCSF Chimera software. HMB was found to be docked in the ligand-binding pocket formed by Ser280, Y314, and H440.

(B) Magnified view of (A) is displayed.

(C) The most stable docked pose of Y314D (mutated) PPARα and HMB was derived from the SwissDock online server. HMB was found to be posed far (>5 Å) from the ligand-binding pocket of Y314D PPARα.

(D) A time-resolved fluorescence resonance energy transfer (TR-FRET) analysis was performed to examine the interaction between PPARα and HMB. The curve was plotted as a 520/490 nm ratio of response with increasing doses of HMB. Curve fit was done in GraphPad Prism software. The analysis generated EC50 (4.02 nM) and Hill slope (0.7949).
(E) TR-FRET was also performed to study the interaction between gemfibrozil (a known ligand of PPARα) and PPARα for comparison.
(F) Thermal shift assay of full-length PPARα was conducted with 10 μM HMB. The melting of PPARα was monitored using an SYBR Green real-time melting strategy.
(G) Thermal shift assay of mutated Y314D-PPARα was also conducted with 10 μM HMB. Results were analyzed and confirmed after three independent experiments.
(H and I) PPARα$^{-/-}$ astrocytes were transduced with either lenti-FL-PPARα or lenti-Y314D-PPARα, and after 48 h of transduction, cells were stimulated wih 10 μM HMB (H). After 6 h, cells were immunostained for PPARα with GFP auto-labeling (I) followed by quantification of MFI of PPARα in six images per group from a total of three independent experiments using the NIH ImageJ. One-way ANOVA followed by Tukey's multiple comparison test was used for statistical analysis.
***$p < 0.001$; NS, not significant.

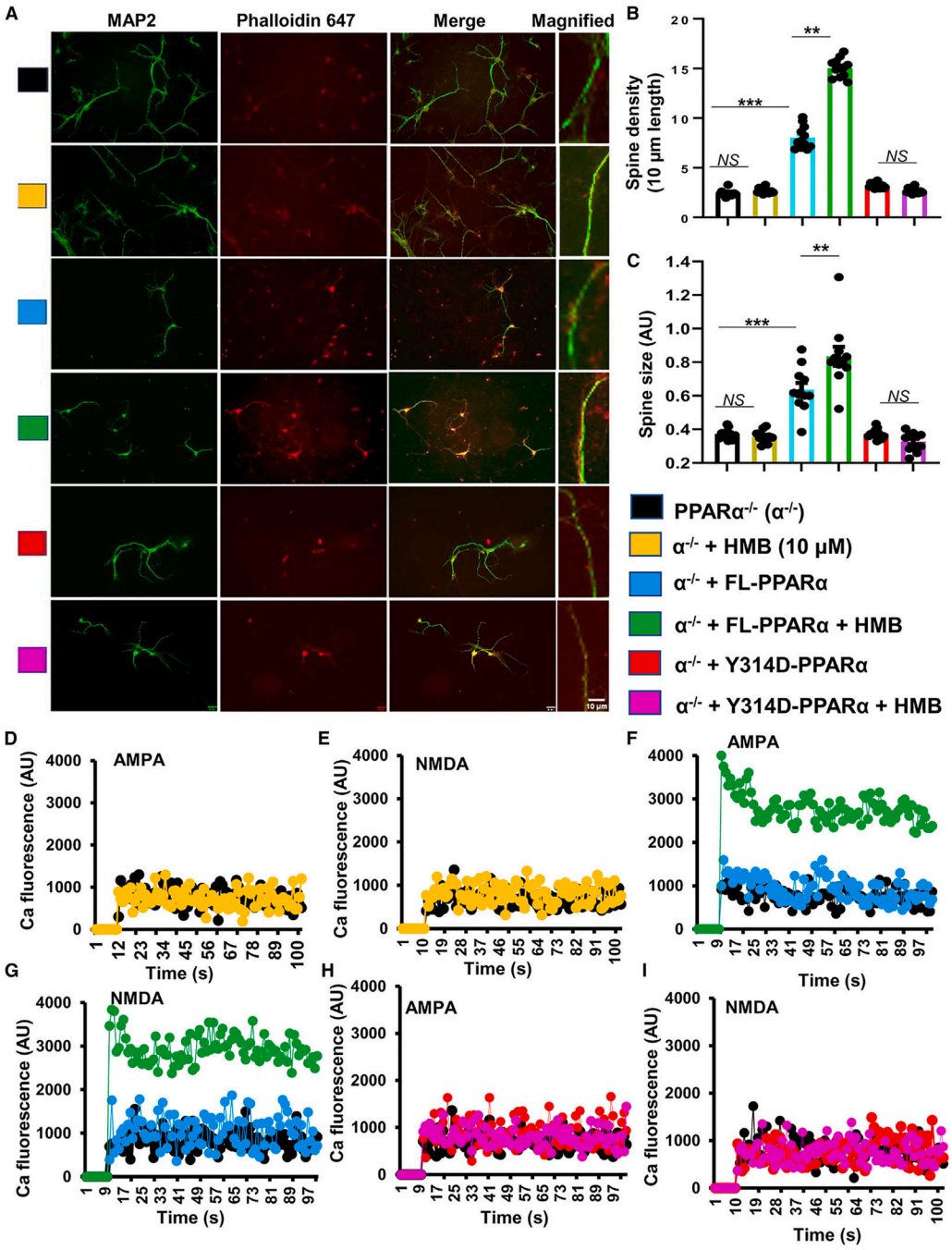

Figure 4. HMB stimulates structural plasticity in hippocampal neurons via PPARα

PPARα$^{-/-}$ embryonic day 18 (E18) hippocampal neurons were transduced with lenti-vector containing either full-length (FL) PPARα or mutated (Y314D) PPARα for 48 h followed by treatment with 10 μM HMB.

(A and B) After 18 h of treatment, cells were double labeled (A) with neuronal marker MAP2 (green) and Alexa 647-conjugated phalloidin (red) in order to stain dendritic spines. (B) Spine density was measured from phalloidin-stained hippocampal neurons and plotted as a function of 10-μm-long dendrites (11 dendrites per each group).

(C) Spine size was also quantified in 11 dendrites per group. Statistical analysis was performed by one-way ANOVA followed by Tukey's multiple comparison test. ***p < 0.001; **p < 0.01; NS, not significant.

(D and E) *PPARα*$^{-/-}$ E18 hippocampal neurons were treated with 10 μM HMB for 18 h followed by analyzing (D) AMPA- and (E) NMDA-driven calcium influx. Results were statistically analyzed by repeated measure two-way ANOVA followed by Tukey's post hoc test. Not significant (p = 0.7166) $\alpha^{-/-}$ vs. $\alpha^{-/-}$ + HMB for AMPA; not significant (p = 0.3609) $\alpha^{-/-}$ vs. $\alpha^{-/-}$ + HMB for NMDA.

(F and G) *PPARα*$^{-/-}$ E18 hippocampal neurons were transduced with lenti-vector containing FL-PPARα for 48 h, treated with 10 μM HMB for 18 h, and assayed for (F) AMPA- and (G) NMDA-driven calcium influx. Results were statistically analyzed by repeated measure two-way ANOVA followed by Tukey's post hoc test. p < 0.001 (= 0.0002) ($\alpha^{-/-}$ + FL-PPARα) vs. ($\alpha^{-/-}$ + FL-PPARα + HMB) for AMPA; p < 0.01 (p = 0.0016) ($\alpha^{-/-}$ + FL-PPARα) vs. ($\alpha^{-/-}$ + FL-PPARα + HMB) for NMDA.

(H and I) *PPARα*$^{-/-}$ E18 hippocampal neurons were transduced with lenti-vector containing Y314D-PPARα for 48 h, treated with 10 μM HMB for 18 h, and assayed for (H) AMPA- and (I) NMDA-driven calcium influx. Results were statistically analyzed by repeated measure two-way ANOVA followed by Tukey's post hoc test. Not significant (p = 0.2727) ($\alpha^{-/-}$ + Y314D-PPARα) vs. ($\alpha^{-/-}$ + Y314D-PPARα + HMB) for AMPA; not significant (p = 0.4910) ($\alpha^{-/-}$ + Y314D-PPARα) vs. ($\alpha^{-/-}$ + Y314D-PPARα + HMB) for NMDA.

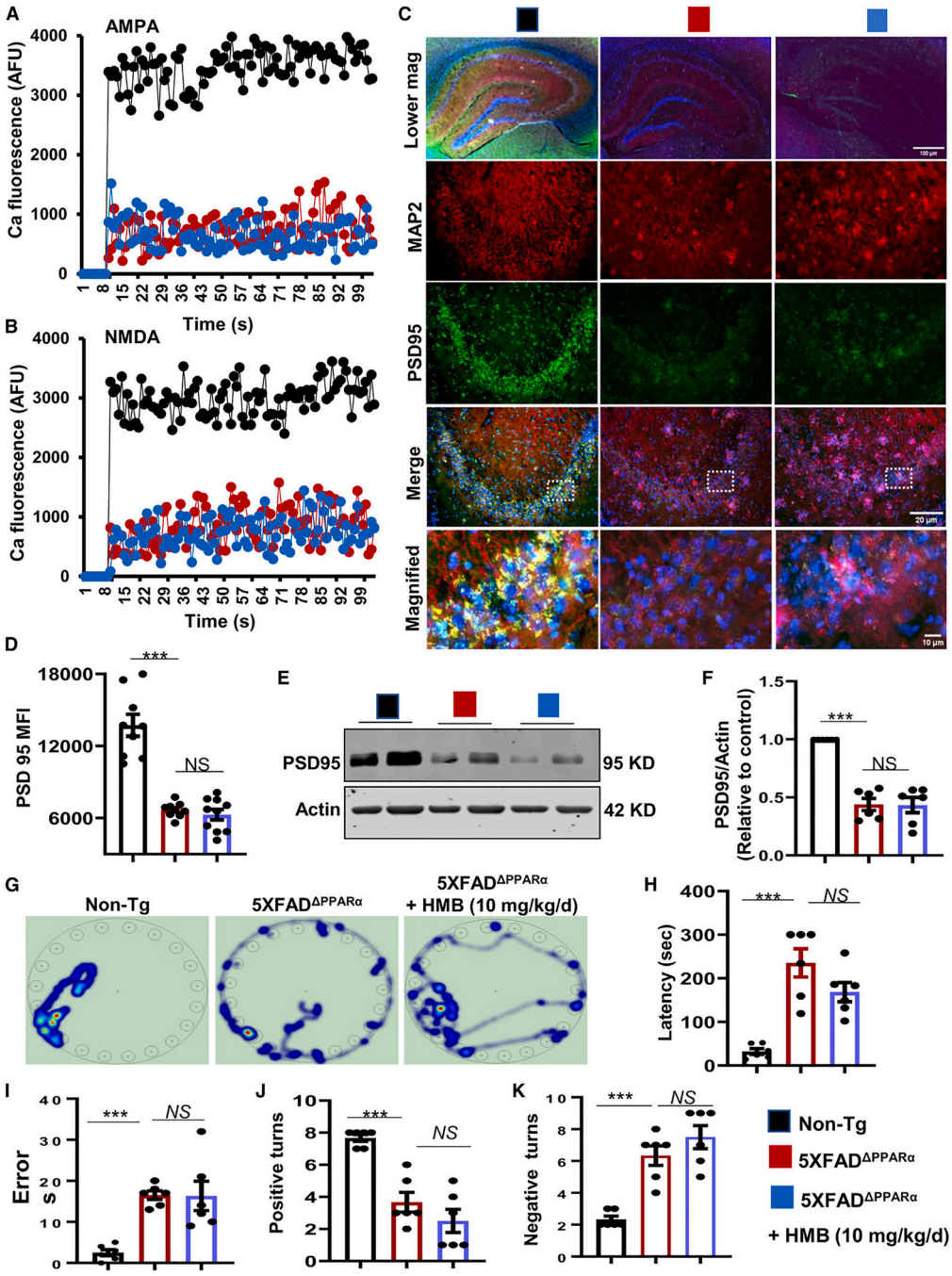

Figure 5. Oral HMB does not improve spatial learning and memory of *5XFAD* mice lacking PPARα

Seven-month-old *5XFAD*$^{\Delta PPARα}$ (*5XFAD* lacking PPARα) mice (n = 6 per group) were treated with HMB (10 mg/kg body wt) via gavage once daily. Since HMB was solubilized in 100 μL water, control *5XFAD* mice also received the same volume of water as vehicle via gavage.

(A and B) After 30 days of treatment, (A) AMPA- and (B) NMDA-dependent calcium currents were measured in the hippocampal slices of different groups of mice. Results were statistically analyzed by repeated measure two-way ANOVA followed by Tukey's post hoc

test. Not significant (p = 0.2071) *5XFAD*$^{\Delta PPAR\alpha}$ vs. *5XFAD*$^{\Delta PPAR\alpha}$+HMB for AMPA; not significant (p = 0.5234) *5XFAD*$^{\Delta PPAR\alpha}$ vs. *5XFAD*$^{\Delta PPAR\alpha}$+HMB for NMDA.

(C and D) Hippocampal sections were double labeled for MAP2 and PSD95 (C) followed by quantification of PSD95 MFI on 10 images from a total of 6 mice per group (D).

(E) Hippocampal extracts were immunoblotted for PSD95.

(F) Bands were scanned and values (PSD95/actin) presented as relative to control. Results are mean ± SEM of six mice per group.

(G–K) After 30 days of treatment, mice were tested for Barnes maze (G, heatmap; H, latency; I, error) and T maze (J, positive turn; K, negative turn). Results are mean ± SEM of six mice per group. One-way ANOVA followed by Tukey's multiple comparison test was used for statistical analysis. ***p < 0.001; NS, not significant.

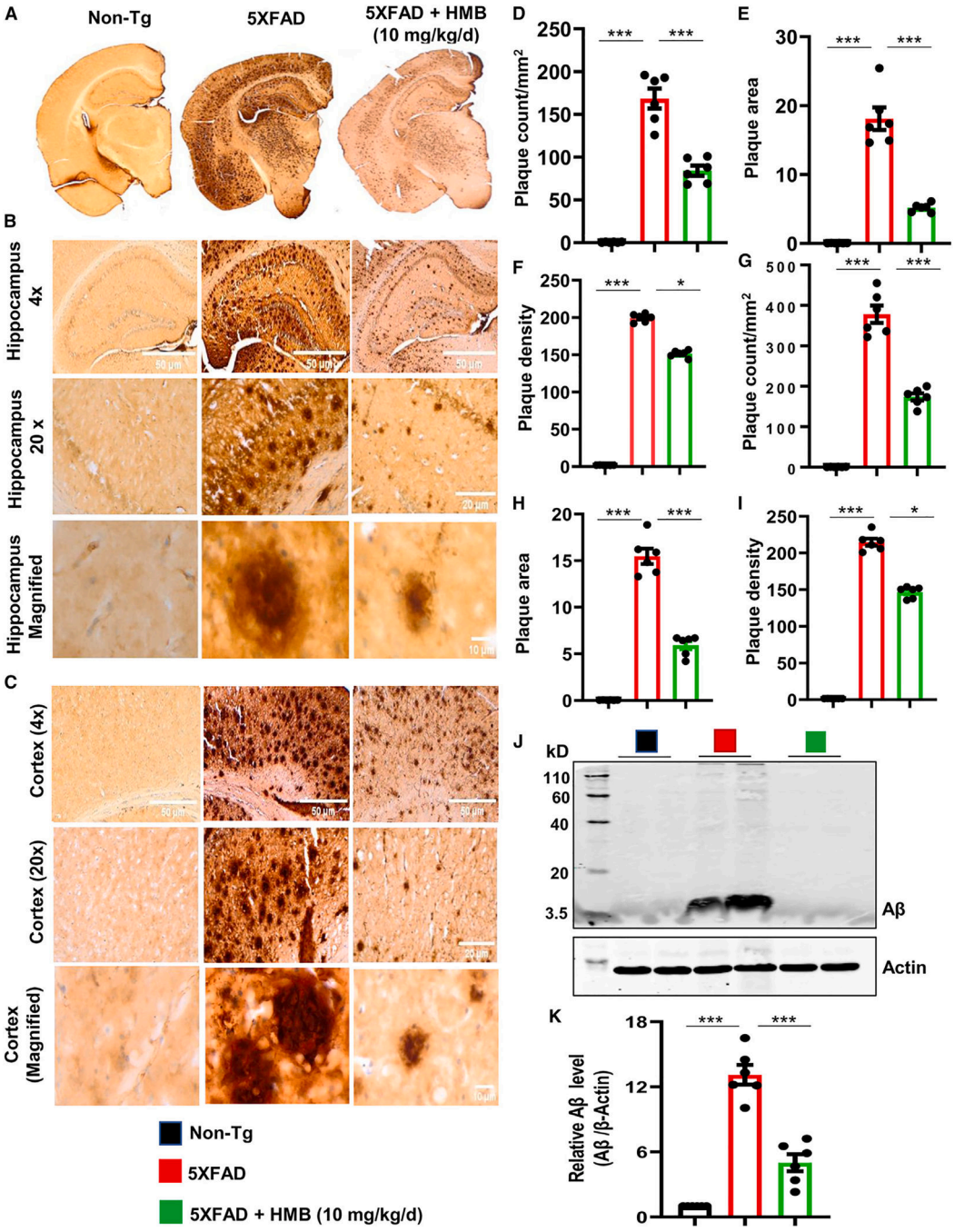

Figure 6. HMB treatment reduces plaque burden in the hippocampus and cortex of *5XFAD* mouse model of AD

Seven-month-old *5XFAD* mice (n = 6 per group) were treated with HMB (10 mg/kg body wt) via gavage once daily. Since HMB was solubilized in 100 μL water, control *5XFAD* mice also received the same volume of water as vehicle via gavage.

(A–I) After 30 days of treatment, hippocampal sections were DAB immunostained with 6E10 antibody (A, lower-magnification [mag] image of the entire section; B, hippocampus of different magnifications; C, cortex of different magnifications; D, number of plaques in the hippocampus; E, area of plaques in the hippocampus; F, density of plaques in the

hippocampus; G, number of plaques in the cortex; H, area of plaques in the cortex; I, density of plaques in the cortex). For quantification, two sections (one image per section) of each of six mice per group were considered. One-way ANOVA followed by Tukey's multiple comparison test was used for statistical analysis. *$p < 0.05$; **$p < 0.01$; ***$p < 0.001$. (J) Hippocampal extracts were immunoblotted for Aβ plaques using 6E10 antibody. (K) Bands were scanned and values (Aβ/actin) presented as relative to control. Results are mean ± SEM of six mice per group. One-way ANOVA followed by Tukey's multiple comparison test was used for statistical analysis. ***$p < 0.001$.

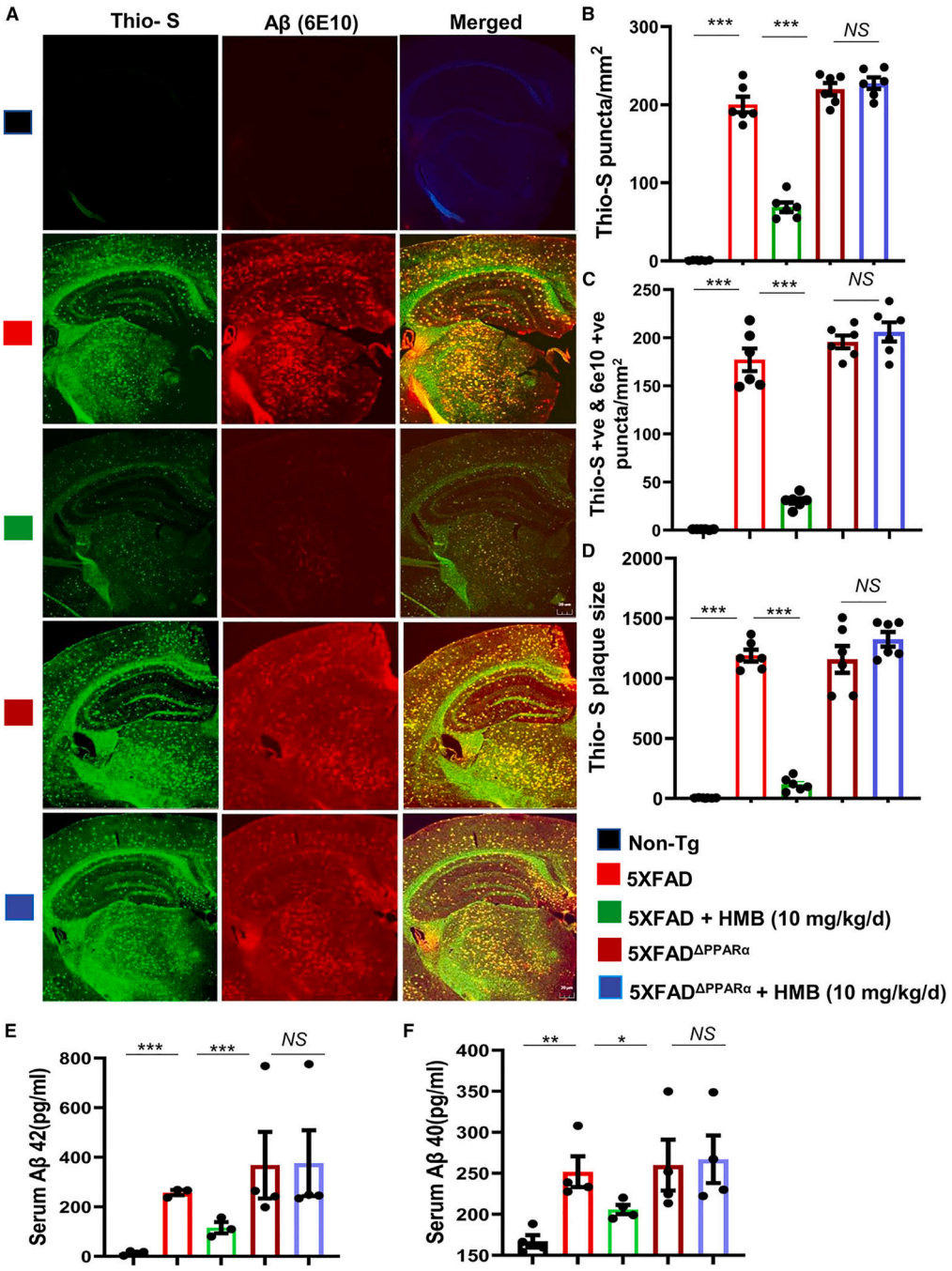

Figure 7. HMB requires PPARα to decrease Ab plaque in the brain of *5XFAD* mice

Seven-month-old *5XFAD* and *5XFADΔPPARα* (*5XFAD* lacking PPARα) mice (n = 6 per group) were treated with HMB (10 mg/kg body wt) via gavage once daily.

Since HMB was solubilized in 100 μL water, control *5XFAD* and *5XFADΔPPARα* mice also received the same volume of water as vehicle via gavage.

(A–D) After 30 days of treatment, hippocampal sections were double labeled with thioflavin-S (green) and 6E10 antibody (red) (A, double-labeled image; B, thioflavin-S [thio-S]-positive area percentage; C, thio-S puncta count; D, thio-S puncta size). For

quantification, two sections (one image per section) of each of six mice per group were considered.

(E and F) Levels of Aβ42 (E) and Aβ40 (F) were quantified in serum by ELISA. One-way ANOVA followed by Tukey's multiple comparison test was used for statistical analysis. ***$p < 0.001$; **$p < 0.01$; *$p < 0.05$; NS, not significant.

KEY RESOURCES TABLE

REAGENT or RESOURCE Antibodies	SOURCE	IDENTIFIER
Antibodies		
SNAP25	Santa Cruz	sc-376713
MAP-2	Millipore	AB5622
BDNF	Abcam	ab203573
CREB	Cell Signaling	#9197
Phospho-Ser133 CREB	Abcam	ab32096
PPARα	Abcam	ab2779
PPARβ	Santa Cruz	sc-7197
NR2A	Cell Signaling	4205S
PSD95	Abcam	ab2723
AP40/AP42	BioLegend	803001
Actin	Abcam	Ab6276
Alexa Fluor 647 AffiniPure Donkey Anti-Rabbit IgG	Jackson ImmunoResearch	711-605-152
Alexa Fluor 488 AffiniPure Donkey Anti-Rabbit IgG	Jackson ImmunoResearch	711-545-152
Alexa Fluor® 647 AffiniPure Donkey Anti-Mouse IgG	Jackson ImmunoResearch	715-605-151
Alexa Fluor 488 AffiniPure Donkey Anti-Mouse IgG	Jackson ImmunoResearch	715-545-150
IRDye 800CW Donkey anti-goat	Li-Cor	926-32214
IR dye 680LT Donkey anti-mouse IgG	Li-Cor	926-68022
Bacterial and virus strains		
Lenti-full-length (FL) PPARα	(Roy et al.)[11,28]	PMID: 27748752
Lenti-Y314D-PPARα	(Roy et al.)[28]	PMID: 27748752
Chemicals, peptides, and recombinant proteins		
β-hydroxy β-methylbutyrate	Sigma	55453
FBS	Atlas	EF-0500-A
DMEM/F12	ThermoFisher	MT10092CV
Neurobasal medium	ThermoFisher	21103049
B-27 supplement	ThermoFisher	17504044
Antibiotic-antimycotic	ThermoFisher	15240062
HEPES	ThermoFisher	15630106
Neurobasal medium, minus phenol red	ThermoFisher	12348017
L-Glutamine	ThermoFisher	A2916801
Poly-D-lysine	Millipore Sigma	P6407-5MG
Critical commercial assays		
Lanthascreen TR-FRET PPARα coactivator assay kit	ThermoFisher	PV4684
pLenti6.3/V5™-TOPO™ TA Cloning™ Kit	ThermoFisher	K531520
ViraPower™ Lentiviral Packaging Mix	ThermoFisher	K497500

REAGENT or RESOURCE Antibodies	SOURCE	IDENTIFIER
FD Rapid Golgistain Kit	FD Neurotechnologies	PK401
Amyloid β 40 ELISA kit	ThermoFisher	KMB3481
Amyloid β 42 ELISA kit	ThermoFisher	KMB3441
Deposited data		
Raw and analyzed data	Figshare	doi: 10.6084/m9.figshare.22825880
Experimental models: Cell lines		
Dissociated mouse hippocampal neurons	This study	N/A
Mouse primary astrocytes	This study	N/A
Experimental models: Organisms/strains		
Mouse: 5XFAD	Jackson Laboratory	(APPwFILon, PSEN1*M146L*L286V)6799Vas/J
Mouse: 5XFAD$^{\Delta PPAR\alpha}$	(Corbett et al.)[29]	PMID: 26080426
Mouse: C57BL/6	Envigo	C57BL/6JOlaHsd
Mouse: PPARα$^{-/-}$	Jackson Laboratoty	B6; 129S4-*Ppara*^{tm1Gonz}/*J*
Mouse: PPARβ$^{-/-}$	(Jana et al.)[49]	PMID: 22879602
Recombinant DNA		
pCMV6-AC-GFP lentiviral backbone expressing TurboGFP	OriGene	PS100010
Mouse PPARα ORF in pCMV6-AC-GFP vector	OriGene	MG 227641
Software and algorithms		
Fiji (ImageJ2)	(Schneider et al.)[50]	PMID: 22930834
Morpheus	Broad Institute	https://software.broadinstitute.org/morpheus/
GraphPad Prism Version 9.5.1 (733)	GraphPad Software Inc.	https://www.graphpad.com/scientific-software/prism/
EthoVision XT video tracking software	BASLER	21743823
Other		
Victor X2 Luminescence spectrometer	Perkin-Elmer	20301379
Victor X5 Luminescence spectrometer	Perkin-Elmer	20301983
Olympus fluorescent microscope	Olympus	BX41
Odyssey Infrared Imaging System	Li-Cor	ODY-1180